AD-A094 812 AIR FORCE INST OF TECH WRIGHT-PATTERSON AFB OH SCHOO--ETC F/G 12/1
MODAL CONTROL OF A SATELLITE IN ORBIT ABOUT L3.(U)
DEC 80 W L SHELTON
UNCLASSIFIED AFIT/GA/AA/80D-3 NL

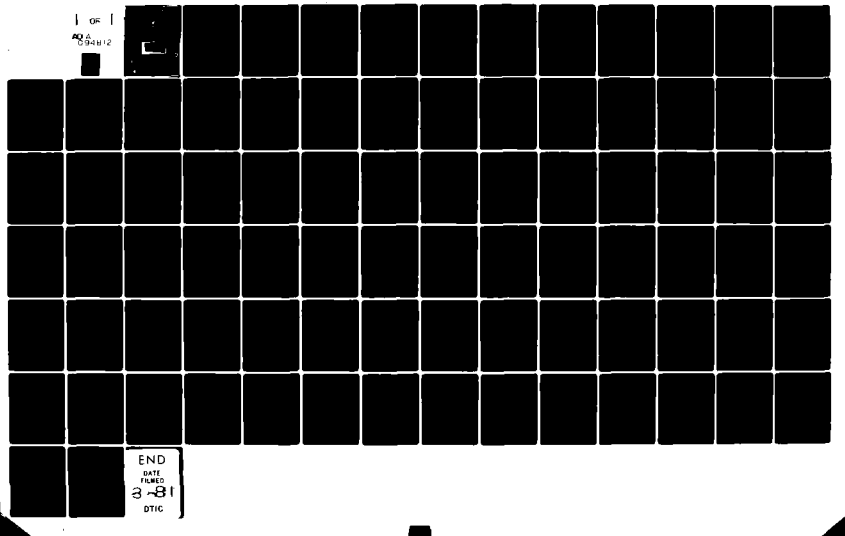

END
DATE FILMED
3-81
DTIC

LEVEL II

AIR FORCE INSTITUTE OF TECHNOLOGY

AIR UNIVERSITY
UNITED STATES AIR FORCE

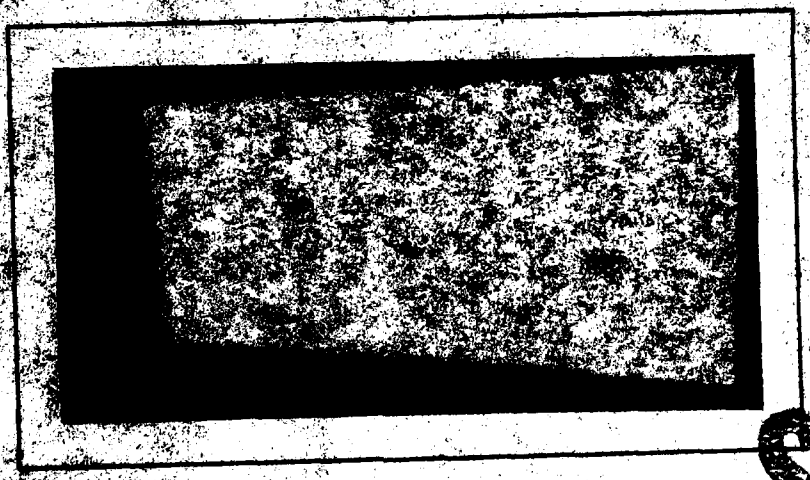

SCHOOL OF ENGINEERING

WRIGHT-PATTERSON AIR FORCE BASE, OHIO

AFIT/GA/AA/80D-3

MODAL CONTROL OF A SATELLITE IN ORBIT ABOUT L3.

THESIS

AFIT/GA/AA/80D-3 William L. Shelton
Captain USAF

Approved for public release; distribution unlimited

AFIT/GA/AA/80D-3

MODAL CONTROL OF A SATELLITE IN ORBIT ABOUT L3

THESIS

Presented to the Faculty of the School of Engineering
of the Air Force Institute of Technology
Air University (ATC)
in Partial Fulfillment of the
Requirements for the Degree of
Master of Science

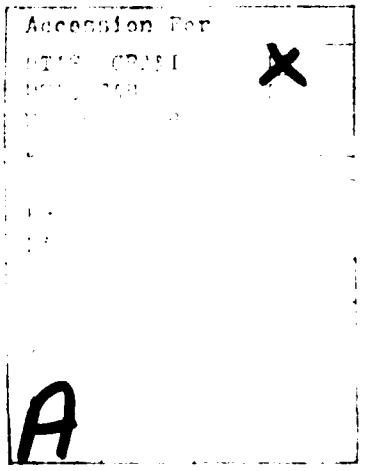

by

William L. Shelton, B.S.
Captain USAF
Graduate Astronautics

December 1980

Approved for public release; distribution unlimited

Acknowledgements

My verbage here is inadequate to express my respect for and appreciation to Dr. Bill Wiesel. He has provided continual encouragement and enthusiasm for this study and has managed to apply guidance to an unguided student. I am deeply indebted to Dr. Wiesel for his constant help and toleration. I will always remember him as a man of great principle and vast knowledge.

My thanks also go out to Dr. Bob Calico and Dr. Jim Silverthorn for their valuable knowledge in the area of modal control. Without their assistance, this work might not have been completed.

I also owe a great deal to Linda for her endurance of these past 18 months. The hours at home were few and my mind was almost never completely at home, but she has provided much loving understanding of my circumstances.

Finally, I can truly say that I owe to God all credit for any accomplishments of this or any work I do. "I can do all things through Christ which strengtheneth me."

Table of Contents

List of Figures

List of Tables

List of Symbols

$\bar{a}$	average control acceleration
A	coefficient matrix of variational system
α	monodromy matrix eigenvalues
B	control matrix
E	total energy of the four-body system
$\bar{E}$	eigenvectors of the four-body system
e	exponentiation
$\bar{f}$	partial dervatives of the kinetic energy
G	universal gravitational constant
H	Hamiltonian of the four-body system
I	identity matrix
J	Jordan form of the matrix of Poincare exponents
k	controller gain
L	Lagrangian of the four-body system
L1-L5	Lagrange points of equilibrium in earth-moon system
Λ	matrix of eigenvectors
λ	Poincare exponents of four-body system
M	sum of the masses of the earth, moon, and sun
m_1	mass of the earth
m_2	mass of the moon
m_3	mass of the sun
m_{SAT}	mass of the satellite

$\bar{\eta}$	modal vector of the four-body problem
p_x, p_y, p_z	momenta of the satellite
Φ	state transition matrix
q_x, q_y, q_z	coordinates of the satellite position
$\bar{R}$	vector from the earth-moon center of mass to the satellite
$r\frac{\cdot}{R}$	time derivative of $\bar{R}$ taken with respect to the rotating reference frame
$\bar{r}$	vector from the earth to the moon
$\bar{r}_{SAT}$	inertial position vector of the satellite
$\bar{\rho}$	vector from the earth-moon center of mass to the sun
$r\frac{\cdot}{\rho}$	time derivative of $\bar{\rho}$ taken with respect to the rotating reference frame
t	time
t_o	initial time
T_{SAT}	Kinetic energy of the satellite
T_s	specific kinetic energy of the satellite
τ	period of orbit about L3
$\bar{u}$	control vector
V_{SAT}	potential energy of the satellite
V_s	specific potential energy of the satellite
$\bar{v}_{SAT}$	velocity vector of the satellite
ω	angular velocity vector of the rotating reference frame
$\bar{x}$	state vector of the four-body system
$\bar{x}_o$	solution state vector

$\bar{x}_{ref}$	state vector along reference orbit about L3
$\Delta\bar{x}$	convergence error state vector
$\delta\bar{x}$	variational state vector

Abstract

A modal control scheme was developed for linear systems that are time periodic. The scheme was then applied to a satellite in orbit about the earth-moon Lagrange point, L3. A theoretical control gain prediction was also devised and then verified by numerical results. The feasibility of the control scheme was then verified by computer simulation by controlling the actual non-linear motions of the satellite with the linearly derived controller. The satellite control costs were found to be 30 percent less than the control costs of a satellite in earth-synchronous orbit.

MODAL CONTROL OF A SATELLITE IN ORBIT ABOUT L3

I. Introduction

Background

Since the advent of spaceflight in the late 1950s and early 1960s, space scientists and mission planners have sought a solution to the problem of maintaining the orbits of sensor-bearing satellites. Coupled with the orbital problem is the desire to use the minimum number of satellites that will satisfactorily accomplish the mission objectives. In the early years of spaceflight, missions were altitude limited by an immature booster technology, but the technology has now matured to the point where virtually any earth orbit is conceivable. A further complication for space scientists is the fact that many space operations such as communications and strategic reconnaisance satellites, require or desire total coverage of the earth's surface by a particular constellation of satellites. Currently, such space operations are conducted by satellites positioned in earth-synchronous orbits, but these satellites do not provide total global coverage. In addition, synchronous orbits are unstable and require the satellites to carry some sort of orbit maintaining device.

The lack of total global coverage is probably the biggest drawback to using synchronous orbits, particularly for communications and reconnaisance applications. Since synchronous orbits are equatorial and the orbits are at an altitude of 35,780 KM (Ref. 6:III-4), placing three satellites in synchronous orbits 120° apart from each other would provide global coverage except for the regions of the north and south poles. The strategic implications of no surveillance or communication in the North Pole region are obvious.

In an era in which the two "superpowers" are developing a space defense capability, it is also important to consider a possible satellite interception. At synchronous altitude, the transfer from the earth's surface to the targeted satellite requires roughly six to eight hours, depending on the launch point of the interceptor, the location of the target, and most importantly the boost capability of the interceptor. This intercept time is extremely short (from a defensive point of view) when one considers that before evasive action can be taken, the defensive forces must determine that the observed launch is in fact an interceptor, the interceptor's target must be identified, and evasive maneuvers (provided the capability exists) must be planned and executed. For future missions of strategic importance, then, earth-synchronous orbits are simply not acceptable.

Attempts to preserve the orbits of satellites have thus far been limited to improvements in control systems. The requirements to carry orbit maintaining devices and orbital stability devices (RCS, momentum wheels, control moment gyros, etc.) can combine to restrict the service life of a satellite in the following manner. Since all launch vehicles that are currently available are thrust limited, they are therefore payload limited. This payload limitation forces a satellite designer to often limit his operational capability. Certainly this problem could be negated if all satellites were launched by a Saturn V booster, but such a plan is neither practical nor economical. From an economic standpoint, a cheaper booster permits a more expensive payload. Due to the weight limitation, it is desirable to allocate the vast majority of available payload weight to the sensors and support equipment required to accomplish the satellite's primary mission. When control systems are required, the weight allocated to the sensors is decreased by the weight of the control systems. When the control system fuel supply is depleted, the satellite's service life is likewise finished. Adding more fuel to extend the service life adds more weight, further decreasing available sensor weight. Currently, all of the above factors combine to force the satellite designer to make design tradeoffs of service life versus mission capability.

If the service life could be extended by decreasing the use of a control system, the designer's job becomes much easier. This leads one to search for higher altitude orbits, since the closer an orbit is to the earth, the faster it decays. Research in the area of such long-term stable orbits gained increased impetus in the 1960s with the initial manned and unmanned explorations of space and consequent discussions of eventual space colonization. Lagrange, in 1772, mathematically demonstrated the existence of equilibrium solutions of the equations of motion for an object located in the Sun-Jupiter system. His theory was finally observationally verified with the discovery of the Trojan group of asteroids in 1906. Together, the Trojan discovery and Lagrange's mathematics demonstrated that there are points in space in the vicinity of two attracting bodies, where the forces on a much smaller mass balance. Assuming the mass of the third body is sufficiently small that it has no effect on the motion of the attracting bodies, the balanced forces cause the third body to be motionless relative to the two attracting bodies. A great deal of research has been accomplished on this "restricted three-body problem" (Ref. 9:231-232).

Since the Trojan discovery, Lagrange's theory has been applied to the earth-moon system and the solution of the mathematics has yielded the five points of equilibrium shown in Figure 1. These five "Lagrange" points (designated L1 through L5) represent theoretical points (in a

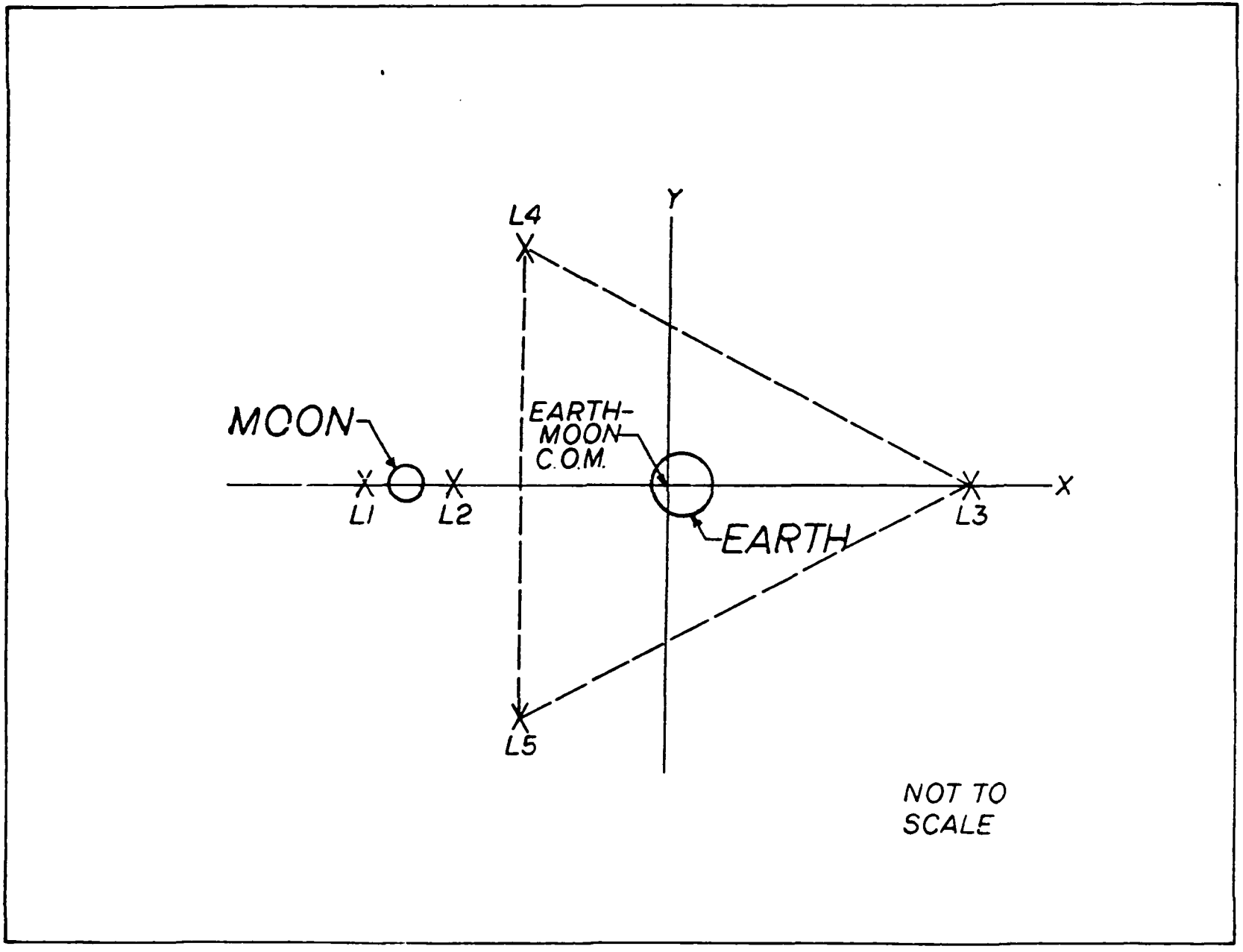

Figure 1. Lagrange Points in Earth-Moon System

coordinate system that rotates with the earth-moon line) in space where an object with zero velocity (relative to the earth and moon) may be placed and the object will remain at that point (which rotates with the frame), thus providing a long-term stable orbit. Motions in the vicinity of the "collinear points", L1, L2, and L3, are inherently unstable, since the eigenvalues of the system equations for the collinear points have at least one eigenvalue with a positive real part (Ref. 7:427). The same analysis shows that the "triangular points", L4 and L5, are inherently stable.

The above theory, though, is based on the restrictive assumptions of circular, planar orbits and does not include the very sizeable perturbations of a fourth body: the sun. When the "restricted four-body problem" (earth, moon, sun, and satellite) is analyzed, the triangular points become unstable and the instabilities of the collinear points become worse. One concludes, then, that the long-term stable orbits at the Lagrangian points do not exist when the more realistic four-body problem is considered. The points do provide, however, a starting reference.

Referring again to Figure 1, note that the points L3, L4, and L5 form an approximately equilateral triangle about the earth. If it were possible, positioning satellites at these three points would provide the desired global coverage of the earth. Since the Lagrange points lie in the earth-moon plane and not the earth-equatorial plane of synchronous orbits, one satellite positioned at each of the

points L3, L4, and L5 would "see" the North Pole at all times.

Problem and Scope

Since the Lagrange points are attractive from a designer's point of view, investigation of the control cost of stabilizing these unstable points is warranted. The yardstick for cost effectiveness must be whether or not the control cost is comparable to the control cost incurred at synchronous altitude. Certainly other factors merit consideration (i.e., additional cost to boost to a higher altitude, advantage of total global coverage, etc.), but this study is limited to the issue of control cost.

Since L4 and L5 were stable prior to the introduction of the perturbative force of the sun, they require less energy to stabilize than L3, which grew even more unstable with the sun's force included. If L3 can be efficiently stabilized, then L4 and L5 should likewise stabilize quite easily. This study, therefore, seeks to stabilize a satellite in the vicinity of L3.

Wiesel used the techniques of Chapter II of this report to construct a periodic orbit about L3, which is shown in Figure 2. The x and y distances of Figure 2 are relative to the origin and axes shown in Figure 1. The orbit was constructed using a "very restricted four-body" model, in which all bodies lie in a plane and the orbits of the earth and moon are circular. Smith (Ref. 8) reconstructed

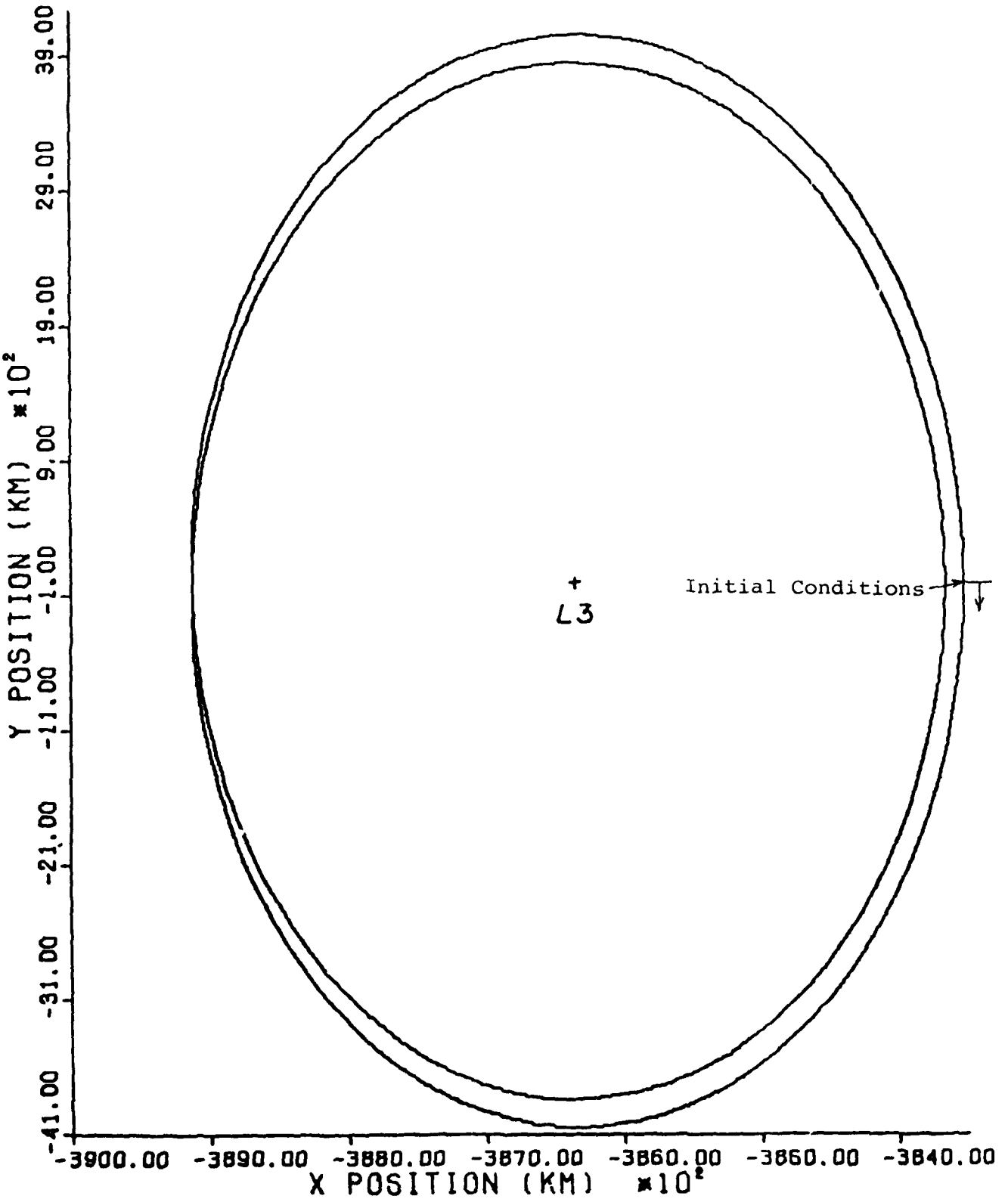

Figure 2. Wiesel Orbit About L3

the Wiesel orbit, found the orbit to be unstable (as expected), and attempted to apply a linear, constant-gain, feedback controller to the satellite displaced from the reference periodic orbit. After attempting various gain magnitudes and various feedback quantities, Smith concluded that the control law was inadequate, based on the control costs he observed.

Smith recommended that follow-on studies use a more realistic model of the four body system and a different control law. This study implements both of these suggestions. The system model was modified in a manner described in the following section and the control law was changed to modal control, also defined in a later section of this report. With the above modifications, a demonstration of the validity of orbits about L3, L4, and L5 for missions requiring a long service life and total global coverage of the earth was initiated.

II. Problem Analysis

Modeling Assumptions

Smith's research was based on a model of the three attracting bodies (earth, moon, and sun) that placed the moon in a circular orbit about the earth with an orbital period of 27.321661 days. The earth's orbit about the sun was also assumed to be circular with a period of 365.256365 days. The model used in this study was changed from the Smith model by placing the moon in an orbit about the earth that is periodic but not circular, as constructed by Wiesel (Ref. 10). The true motion of the moon about the earth is not actually periodic, but the Wiesel lunar orbit more closely describes the actual motion of the moon. The earth orbit about the sun was still modelled as circular with the same orbital period used by Smith. Other inclination and eccentricity effects were initially ignored in this study, thereby restricting the motions of the four bodies to a plane.

Coordinate System

The derivation of the four-body problem Hamiltonian, which is described in the following section, is accomplished with respect to the coordinate system shown in Figure 3. Research by Heppenheimer (Ref. 5) and others has shown that the periodicity of the orbit about L3 is not

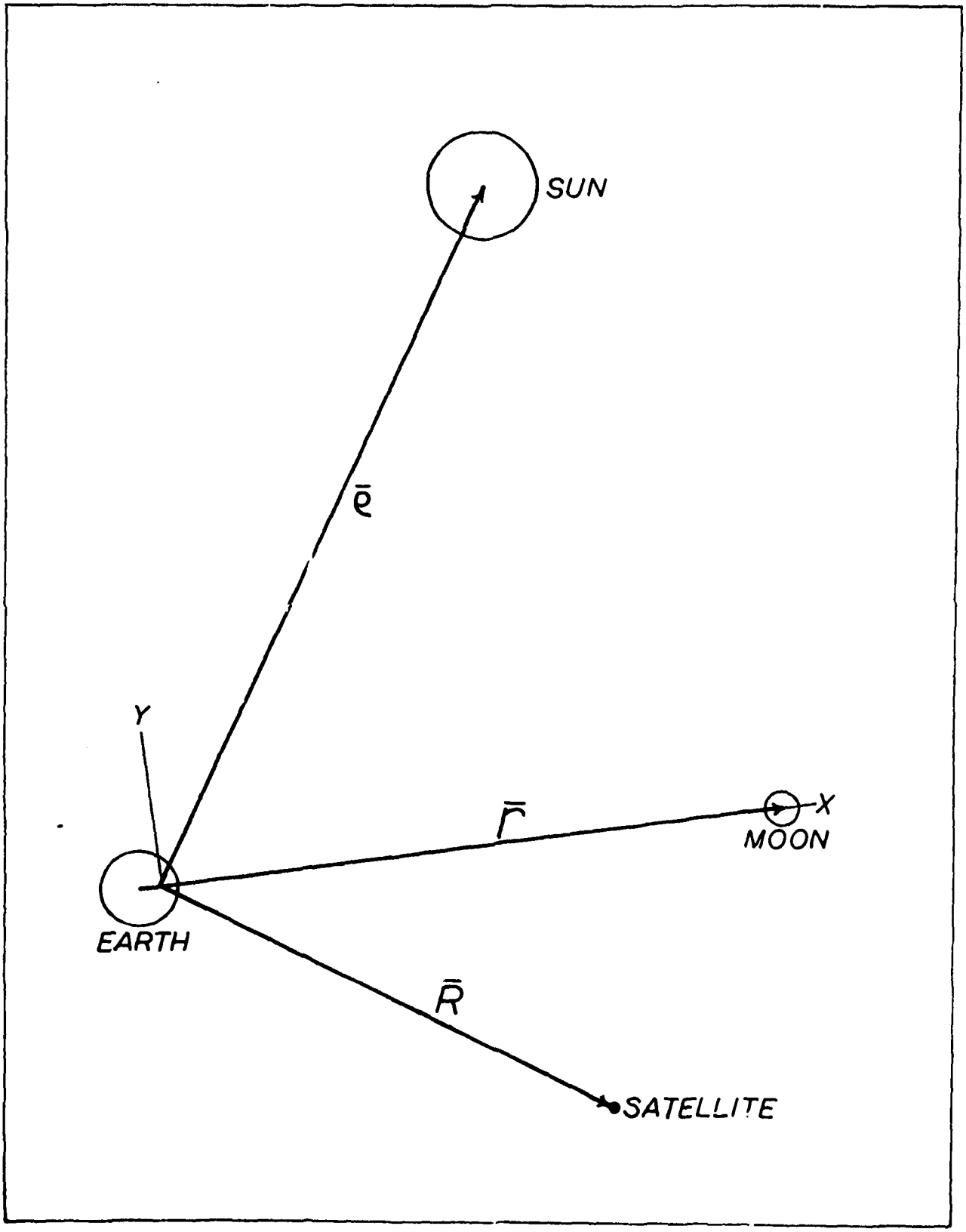

Figure 3. Geometry of the Four-Body Problem

readily apparent in inertial or pseudo-inertial coordinates; therefore, the coordinate system chosen for this study rotates with an angular velocity equal to the average angular velocity of the moon, and the center of the system is located at the earth-moon center of mass. This frame allows easy visualization of the periodic nature of the orbit about L3.

Derivation of the Hamiltonian

To properly derive the dynamics for the restricted four-body problem, the three attracting bodies were assumed to have their actual masses while the satellite shown in Figure 3 (to be later positioned on the L3 orbit) was assumed to be massless (as in the restricted three-body problem). This assumption assures that the attracting bodies dictate the motion of the satellite, but the satellite has no effect on the motion of the attracting bodies.

As in the derivation of any Hamiltonian, the kinetic and potential energies were first constructed. The inertial point in this derivation was assumed to be the earth-moon-sun center of mass, which allows the inertial position vector of the satellite to be written

$$\bar{r}_{SAT} = \bar{R} - \frac{m_3}{M} \bar{\rho} \qquad (1)$$

where $M = m_1 + m_2 + m_3$ (sum of the masses of the earth, moon, and sun, respectively) and the scale factor $\frac{m_3}{M}$ locates the inertial point of the system. Taking the

inertial time derivative of the position vector in the rotating frame yields

$$\frac{r_d}{dt}(r_{SAT}) = \bar{v}_{SAT} = \dot{\bar{R}}^r + (\bar{\omega}x\bar{R}) + (-\frac{m_3}{M})\dot{\bar{\rho}}^r + \bar{\omega}x(-\frac{m_3}{M})\bar{\rho} \quad (2)$$

where $-\frac{m_3}{M}\dot{\bar{\rho}}^r + \bar{\omega}x(-\frac{m_3}{M})\bar{\rho}$ is the transport velocity of the earth-moon center of mass. The symbol $\bar{\omega}$ denotes the angular velocity vector of the rotating frame, which is actually the moon's mean inertial angular velocity vector, and the superscript r represents differentiation in the rotating frame. Kinetic energy is defined as

$$T_{SAT} = \tfrac{1}{2}\, m_{SAT}\, (\bar{v}_{SAT} \cdot \bar{v}_{SAT}) \quad (3)$$

But since the satellite is assumed to be massless, the mass is divided from both sides to yield the specific kinetic energy, T_s.

$$\begin{aligned} T_s = \tfrac{1}{2}\{ & \dot{\bar{R}}^r \cdot \dot{\bar{R}}^r + (\bar{\omega}x\bar{R})\cdot(\bar{\omega}x\bar{R}) + \dot{\bar{\rho}}^r \cdot \dot{\bar{\rho}}^r \\ & + (\bar{\omega}x\tfrac{m_3}{M}\bar{\rho})\cdot(\bar{\omega}x\tfrac{m_3}{M}\bar{\rho}) + 2[\dot{\bar{R}}^r\cdot(\bar{\omega}x\bar{R})] \\ & + 2(\dot{\bar{R}}^r\cdot\tfrac{m_3}{M}\dot{\bar{\rho}}^r) + 2[\dot{\bar{R}}^r\cdot(\bar{\omega}x\tfrac{m_3}{M}\bar{\rho})] \\ & + 2[(\bar{\omega}x\bar{R})\cdot\tfrac{m_3}{M}\dot{\bar{\rho}}^r] + 2[(\bar{\omega}x\bar{R})\cdot(\bar{\omega}x\tfrac{m_3}{M}\bar{\rho})] \\ & + 2[\tfrac{m_3}{M}\dot{\bar{\rho}}^r\cdot(\bar{\omega}x\tfrac{m_3}{M}\bar{\rho})]\} \end{aligned} \quad (4)$$

The potential energy, V, of the satellite is due to the gravitational attraction of the other three bodies and has the form

$$V_{SAT} = \sum_{i=1}^{3} \frac{-Gm_i m_{SAT}}{r_{i\text{-}SAT}} \quad (5)$$

where $r_{i\text{-SAT}}$ is the magnitude of radius vector from the i^{th} body to the satellite and G is the universal gravitational constant. As in the case of the kinetic energy, we construct a specific potential energy by dividing both sides of (5) by m_{SAT}.

$$V_s = \frac{-Gm_3}{|\bar{R} - \bar{\rho}|} - \frac{Gm_1}{|\frac{m_2}{m_1+m_2}\bar{r} + \bar{R}|} - \frac{Gm_2}{|\bar{R} - \frac{m_1}{m_1+m_2}\bar{r}|} \tag{6}$$

Since potential energy is not dependent on rate terms (time derivatives of the coordinates), the momenta, p_i, of the Hamiltonian can be written

$$p_i = \frac{\partial T_s}{\partial \dot{q}_i} \qquad i = 1, 2, 3 \tag{7}$$

where $\dot{q}_i$ is the time derivative of the i^{th} coordinate. Coordinates chosen were the x, y, and z components of the satellite's position in the coordinate frame of Figure 3 (R_x, R_y, and R_z). In this coordinate frame, the p_i are actually inertial velocity components, a distinction that became very important for the derivation of the controller.

The full Hamiltonian, then, is given by

$$H = \sum_{i=1}^{3} p_i\dot{q}_i - L = \sum_{i=1}^{3} p_i\dot{q}_i - T + V \tag{8}$$

With algebraic simplification of the above equation after all terms were included, the Hamiltonian reduces to

$$\begin{aligned} H = {} & \tfrac{1}{2}(p_x^2 + p_y^2 + p_z^2) + \omega(p_xR_y - p_yR_x) \\ & + \frac{m_3}{M}[(\dot{r}\rho_x - \omega\rho_y)p_x + (\dot{r}\rho_y + \omega\rho_x)p_y] \\ & - \frac{Gm_3}{|\bar{R}-\bar{\rho}|} - \frac{Gm_1}{|\frac{m_2}{m_1+m_2}\bar{r}+\bar{R}|} - \frac{Gm_2}{|\bar{R} - \frac{m_1}{m_1+m_2}\bar{r}|} \end{aligned} \tag{9}$$

Since the motion of the earth about the sun was assumed to be planar, no z component of $\bar{\rho}$ exists in the Hamiltonian.

Construction of the Periodic Orbit

Equations of motion are formed in Hamiltonian systems by forming

$$\dot{q}_k = \frac{\partial H}{\partial p_k} \qquad k = 1, 2, \ldots, n \tag{10}$$

$$\dot{p}_k = \frac{-\partial H}{\partial q_k} \qquad k = 1, 2, \ldots, n \tag{11}$$

where n represents the number of generalized coordinates describing the system (Ref. 7:94). To generalize, these equations can be rewritten as

$$\dot{\bar{x}}(t) = \bar{f}(\bar{x}(t),t) \tag{12}$$

where $\bar{x}$ is a state vector, and for this study is composed of the coordinates and momenta of the system. The vector $\bar{f}$ contains the partial derivatives described by (10) and (11), and is a function of both the states and time.

The goal of a search for a periodic orbit, then, is to find a solution to (12) that closes on itself in a finite amount of time. The time from the initial starting position until the orbit closes on itself is defined as an orbital period and is denoted by τ. The motion from τ to 2τ in a periodic system should be a repeat of the motion from 0 to τ. In the restricted problem of three bodies, the Hamiltonian itself is a constant of the motion, which results in a continuous family of orbits about the five

equilibrium points. This is not the case, however, in the restricted four-body problem, since the Hamiltonian becomes an explicit function of time. If periodic orbits about the equilibrium points still exist in the four-body problem, one would expect the orbits to have a one to one resonance with the motion of the moon. Unpublished research by Wiesel has confirmed that the one to one resonance condition does apply to orbits about the earth-moon Lagrange points.

Assuming the existence of a periodic solution to (12), $\bar{x}_o(t)$, over a given time interval, a small displacement, $\delta\bar{x}$, may be added at the initial time, t_o. The displaced solution can then be expanded in a Taylor series about the solution $\bar{x}_o(t)$ to yield

$$\bar{x}(t) = \bar{x}_o(t) + \frac{\partial \bar{x}(t)}{\partial \bar{x}(t_o)} \Bigg|_{\bar{x}_o(t)} \delta\bar{x}(t_o) + \text{higher order terms} \quad (13)$$

Truncating (13) at first order and defining

$$\delta\bar{x}(t) = \bar{x}(t) - \bar{x}_o(t) \quad (14)$$

one obtains

$$\delta\bar{x}(t) = \Phi(t,t_o)\delta\bar{x}(t_o) \quad (15)$$

a variational equation for the system where

$$\Phi(t,t_o) = \frac{\partial \bar{x}(t)}{\partial \bar{x}(t_o)} \Bigg|_{\bar{x}_o(t)} \quad (16)$$

The matrix, Φ, is termed the state transition matrix and is a function of only the initial and final times being considered. The nxn Φ matrix has the properties

$$\Phi(t.t_o) = \Phi(t,t_1)\Phi(t_1,t_o) \tag{17}$$

and

$$\Phi(t_o,t_o) = I \tag{18}$$

where I is the nxn identity matrix.

For the variational equation, (15), to be of value, a differential equation for the propagation of $\delta\bar{x}(t)$ must be derived. Referring to the equations of motion, (12), and the equation for $\delta\bar{x}(t)$, (14) one can form the equation

$$\dot{\bar{x}}_o(t) + \delta\dot{\bar{x}}(t) = \bar{f}(\bar{x}_o(t) + \delta\bar{x}(t),t) \tag{19}$$

This equation can also be expanded in a Taylor series about $\bar{x}_o(t)$ to yield

$$\dot{\bar{x}}_o(t) + \delta\dot{\bar{x}}(t) = \bar{f}(\bar{x}_o(t),t) + \frac{\partial\bar{f}}{\partial\bar{x}(t)}\Big|_{\bar{x}_o(t)} \bar{x}(t) + \text{higher order terms} \tag{20}$$

Substituting Equation (12) into (20) produces

$$\delta\dot{\bar{x}}(t) = A(t)\delta\bar{x}(t) \tag{21}$$

to first order, where

$$A(t) = \frac{\partial\bar{f}}{\partial\bar{x}(t)}\Big|_{\bar{x}_o(t)} \tag{22}$$

Differentiating (15) with respect to time yields

$$\delta\dot{\bar{x}}(t) = \dot{\Phi}(t,t_o)\delta\bar{x}(t_o) \tag{23}$$

since $\delta\bar{x}(t_o)$ is a constant. Equating (21) and (23) one obtains

$$\dot{\Phi}(t,t_o)\delta\bar{x}(t_o) = A(t)\delta\bar{x}(t) \tag{24}$$

But $\delta\bar{x}(t)$ is defined by (15), and substituting for $\delta\bar{x}(t)$ produces

$$\dot{\Phi}(t,t_o)\delta\bar{x}(t_o) = A(t)\Phi(t,t_o)\delta\bar{x}(t_o) \tag{25}$$

$$\dot{\Phi}(t,t_o) = A(t)\Phi(t,t_o) \tag{26}$$

Numerically integrating equations (12) and (26) simultaneously with chosen initial conditions for $\bar{x}(t_o)$ and initial conditions for Φ defined by (18), one obtains information on the solution $\bar{x}_o(t)$ and its local variation.

The initial conditions chosen for $\bar{x}(t_o)$ are actually an educated guess at the initial conditions for the actual orbit. Integrating with these initial conditions over a period, τ, one obtains $\bar{x}_o(\tau)$ and $\Phi(\tau,0)$. Since $\bar{x}(t_o)$ was merely a guess, iteration will be required to find the actual orbit and accompanying initial conditions. The error between the initial conditions and the value of the states after integrating over τ is expressed as

$$\Delta\bar{x} = \bar{x}_o(\tau) - \bar{x}_o(0) \tag{27}$$

If the initial conditions are varied by $\delta\bar{x}(0)$, the resultant $\delta\bar{x}(\tau)$ will not necessarily produce the sought periodic orbit; however, if we let

$$\delta\bar{x}(0) = \delta\bar{x}(\tau) - \Delta\bar{x} \tag{28}$$

the periodic orbit will be produced. Recalling (15) once again and substituting it into (28) yields

$$\Delta\bar{x} = \Phi(\tau,0)\delta\bar{x}(0) - \delta\bar{x}(0) \tag{29}$$

$$\Delta\bar{x} = [\Phi(\tau,0) - I]\delta\bar{x}(0) \tag{30}$$

The above vector equation can be viewed as a linear equation for $\delta\bar{x}(0)$ in terms of the known quantities $\Delta\bar{x}$, $\Phi(\tau,0)$, and I. If the higher order terms of (13) and (20) were included in the derivation, only one iteration step would be required for convergence; however, the linearization of the two equations forces an iteration until the solution converges to a chosen tolerance.

Implementation of the Theory

Using the theory of the previous section, a new periodic orbit about L3 was constructed. Equations (12) and (26) were numerically integrated simultaneously over one orbital period and the $\Delta\bar{x}$ was computed. Since the system model was modified only slightly from the Smith orbit, his initial conditions were used to start the iteration (Ref 8). The $\Delta\bar{x}$ was used in the correction equation (30) to adjust the initial conditions and the calculations were repeated until convergence. The final convergence error chosen for the orbit was 1×10^{-10}, which is also the accuracy of the integration routine supplied by Wiesel. Once the orbit was

found, a Fourier series (Ref. 2:60) was fit to each of the states of the orbit (which were calculated at evenly spaced points around the orbit), with a resulting nineteen coefficient Fourier series representation of the orbit. The purpose of the Fourier series representation was to easily store a reference orbit for control analysis (described in Chapter IV of this report). The new orbit is shown in Figure 4. Again, the x and y positions shown in Figure 4 are relative to the earth-moon center of mass, previously defined as the origin of the coordinate system (Figure 3). When the new orbit is compared to the Wiesel orbit, one notices very little difference between the two. As previously stated, the only difference in the construction of the two orbits are the two models of the moon. The addition of the periodic versus the circular orbit for the moon resulted in a slightly smaller orbit in both x and y directions. The initial conditions for the Wiesel orbit and the new orbit are shown in Table I.

TABLE I. L3 Orbit Initial Conditions

	Wiesel Orbit	New Orbit
x position (km)	-383,519.08	-383,537.27
y position (km)	0.0	0.0
z position (km)	0.0	0.0
x momentum (km/sec)	0.0	0.0
y momentum (km/sec)	-30.825652	-30.825537
z momentum (km/sec)	0.0	0.0

Figure 4. New Orbit About L3

III. Floquet Solution for the Periodic System

Floquet Theory

Unlike the restricted three-body problem Hamiltonian, the four-body problem Hamiltonian is an explicit function of time. Consequently, the Hamiltonian itself is no longer a constant of the motion. Certainly energy is conserved ($T + V = E = \text{constant}$), but no other constants of the motion exist (Ref 7:416). The equations of motion derived from the four-body Hamiltonian are also found to be time-varying but periodic, as one would expect since the problem at hand is an orbital problem. Repeating (21), the variational equations of motion may be written in general state vector form as

$$\dot{\delta\bar{x}}(t) = A(t)\delta\bar{x}(t) \tag{31}$$

The periodicity of the system is contained in the coefficient matrix A(t) such that

$$A(t) = A(t+\tau) \tag{32}$$

where τ is once again defined as the period of the system. Differential equations such as (31), which have variable yet periodic coefficients can theoretically be reduced to the case of constant coefficient, linear differential

equations, by the theory of Floquet (Ref 4:60). Floquet's theory states that the general solution to (31) is of the form

$$\delta\bar{x}(t) = \sum_{j=1}^{n} \beta_j \bar{E}_j(t) e^{\lambda_j t} \tag{33}$$

where β_j and λ_j are constants and the $\bar{E}_j$ are periodic functions of time with the same orbital period, τ. Actually, (33) represents a special case solution where the λ_j are all multiplicity one. The n λ_j can be arranged in a matrix of Jordan canonical form as shown below (Ref 7:267).

$$J = \begin{bmatrix} \lambda_1 & & & [0] \\ & \lambda_2 & & \\ & & \ddots & \\ & & & \\ [0] & & & \lambda_n \end{bmatrix} \tag{34}$$

Previous work by Smith and Wiesel had verified the simple multiplicity of the λ_j; therefore, the assumption of the form of (33) is warranted. The constant λ_j is called a characteristic exponent or Poincare exponent and the quantity $e^{\lambda_j t}$ is termed a characteristic multiplier of A(t). What follows is a method for computing $\bar{E}_j$ and λ_j.

Assuming one desires to excite only one mode of the system (31), let $\beta_j = 0$ for $j \neq i$ and $\beta_i = 1$ which, from (33), yields

$$\delta\bar{x}(t) = \bar{E}_i(t) e^{\lambda_i t} \tag{35}$$

From (15),

$$\delta\bar{x}(t) = \Phi(t,0)\delta\bar{x}(0) \tag{36}$$

Equating (35) and (36), one obtains

$$\bar{E}_i(t)e^{\lambda_i t} = \Phi(t,0)\delta\bar{x}(0) \tag{37}$$

$$= \Phi(t,0)\bar{E}_i(0) \tag{38}$$

Since $\bar{E}_i(t)$ has already been defined as a periodic vector, $\bar{E}_i(\tau) = \bar{E}_i(0)$, such that

$$\delta\bar{x}(\tau) = \bar{E}_i(\tau)e^{\lambda_i \tau} \tag{39}$$

$$= \bar{E}_i(0)e^{\lambda_i \tau} = \Phi(\tau,0)\bar{E}_i(0) \tag{40}$$

Rearranging (40) yields the eigenvalue problem

$$\{\Phi(\tau,0) - (e^{\lambda_i \tau})I\}\bar{E}_i(0) = \bar{0} \tag{41}$$

$\Phi(\tau,0)$ is called the monodromy matrix and its eigenvalues are $e^{\lambda\tau}$. Defining the monodromy matrix eigenvalues as α_i, the Poincare exponents can be found by

$$\lambda_i = \frac{1}{\tau} \ln(\alpha_i) \tag{42}$$

The eigenvectors of $\Phi(\tau,0)$, therefore, are the vectors $\bar{E}_i(0)$.

To compute the complete solution, $\bar{E}_i(t)$ must be computed over an entire period. Since $\bar{E}_i(t)$ is periodic, determining $\bar{E}_i(t)$ over one period determines the vector for all time. Recalling (35) and (31), one can write

$$\frac{d}{dt}(\bar{E}_i(t)e^{\lambda_i t}) = \Lambda(t)(\bar{E}_i(t)e^{\lambda_i t}) \tag{43}$$

Now define $\Lambda(t)$ as the square matrix composed of the n $\bar{E}_i(t)$ partitioned into columns

$$\Lambda(t) = [\bar{E}_i(t)|\bar{E}_2(t)|\ldots|\bar{E}_n(t)] \tag{44}$$

Now, by the form of (43) and the above definition, one can show that

$$\dot{\Lambda}(t)\, e^{Jt} + \Lambda(t)Je^{Jt} = A(t)\Lambda(t)e^{Jt} \tag{45}$$

$$\dot{\Lambda}(t) + \Lambda(t)J = A(t)\Lambda(t) \tag{46}$$

The above equation provides an ordinary differential equation for Λ. with initial conditions $\bar{E}_i(0)$, previously defined as the eigenvectors of $\Phi(\tau,0)$.

One can also define a new variable $\xi(t)$ such that

$$\xi(t) = \Lambda(t)e^{Jt} \tag{47}$$

and from (45)

$$\dot{\xi}(t) = A(t)\xi(t) \tag{48}$$

The initial condition, $\xi(0)$, for this equation is the $\bar{E}_i(0)$ arranged in columns or $\Lambda(0)$. This equation has the same form as the differential equation for Φ, (26), which verfies that ξ is, in fact, Φ, to within a coordinate rotation.

Implementation of the Theory

After finding the Fourier series representation of the orbit, the stability of the orbit was investigated.

Using the theory of the previous section, the system eigenvectors and Poincare exponents were found from the eigenvalue problem of (41) combined with (42). The monodromy matrix was produced by integrating (26) when the periodic orbit was found.

Smith's analysis of the Wiesel orbit (Ref 8) demonstrated that the Wiesel orbit is unstable, and the analysis of the new orbit indicates the same instability. As predicted, one of the system's Poincare exponents is a positive real root (conjugate root is negative and real), while the other roots are pure complex conjugates. Table II below demonstrates the slight differences between the Poincare exponents of the two orbits.

Table II. Poincare Exponents of the Two Orbits (i-imaginary)

Mode	Poincare Exponent	
	Wiesel Orbit	New Orbit
Planar Mode	0.0 - 1.0398i	0.0 - 1.0392i
	0.0 + 1.0398i	0.0 + 1.0392i
Planar Mode	2.3932 + 0.0i	2.3921 + 0.0i
	-2.3932 + 0.0i	-2.3921 + 0.0i
Out of Plane Mode	0.0 - 1.1248i	0.0 - 1.1247i
	0.0 + 1.1248i	0.0 + 1.1247i

In both orbits, the unstable exponent of the system is designated λ_3 and is the root the controller must change.

IV. Control Theory

Review of Previous Work

Previous work by Wiesel and Smith demonstrated that there are three modes of oscillation for the periodic orbit about L3. Two of the modes lie in the orbit plane while the third mode is out of the plane. Wiesel and Smith also discovered that the out-of-plane mode and one of the planar modes were stable yet the other planar mode was unstable, thereby necessitating some form of control on the satellite in orbit about L3. Smith attempted feedback control, attempting both rate and position feedback laws. This scheme was unsuccessful due to the fact that all modes were excited by the control, which is contrary to the desired effect of the control affecting only the unstable mode. Exciting all modes resulted in control costs that were significantly higher than the costs of satellites in earth-synchronous orbits. Obviously, then, an alternate control scheme that does not excite the two stable modes must be implemented.

Modal Control

The basic premise of modal control is to perform control on a preselected number of system modes without exciting the remaining modes of the system. In terms of classical control theory, modal control can be viewed as a

pole placement technique. The instabilities of the system caused by roots lying in the right-half of the complex plane, are removed via the controller moving the unstable roots from the right-half to the left-half of the complex plane. Simultaneously, the other system roots remain in their original locations in the complex plane.

Since the Poincare exponents of Hamiltonian systems are always conjugate pairs, the one unstable mode of the four-body problem implies a pair of roots on the real axis: one root in the right-half-plane, the conjugate root in the left-half-plane. The goal, then, of the modal control applied to this problem was to move the one root out of the right-half-plane while the other five roots remained at their original locations in the complex plane. The derivation of the controller follows.

To apply control to the system, (31) must be augmented to yield the state equation

$$\dot{\delta\bar{x}}(t) = A(t)\delta\bar{x}(t) + B(t)\bar{u}(t) \tag{49}$$

where $\bar{u}(t)$ is the control vector and B(t) determines to what states control is applied, i.e. B(t) represents the physical reality of the control. To insure that any control applied to the system affects only the mode of interest, the system must be transformed to a diagonal set of equations. To accomplish this objective, define a new variable

$$\bar{\eta}(t) = \Lambda^{-1}(t)\delta\bar{x}(t) \tag{50}$$

where $\bar{\eta}$ is termed the modal vector.

Taking the time derivative of the above equation yields

$$\dot{\delta\bar{x}}(t) = \dot{\Lambda}(t)\bar{\eta}(t) + \Lambda(t)\dot{\bar{\eta}}(t) \tag{51}$$

Equating (49) and the above equation

$$\dot{\Lambda}(t)\bar{\eta}(t) + \Lambda(t)\dot{\bar{\eta}}(t) = A(t)\delta\bar{x}(t) + B(t)\bar{u}(t) \tag{52}$$

$$= A(t)\Lambda(t)\bar{\eta}(t) + B(t)\bar{u}(t) \tag{53}$$

Solving for $\bar{\eta}$, since a differential equation for propagation of the modes is desired, yields

$$\dot{\bar{\eta}}(t) = \Lambda^{-1}(t)[A(t)\Lambda(t) - \dot{\Lambda}(t)]\bar{\eta}(t) + \Lambda^{-1}(t)B(t)\bar{u}(t) \tag{54}$$

From (46) of the previous chapter,

$$\dot{\Lambda}(t) = A(t)\Lambda(t) - \Lambda(t)J \tag{55}$$

and substitution into (54) above produces

$$\dot{\bar{\eta}}(t) = J\bar{\eta}(t) + \Lambda^{-1}(t)B(t)\bar{u}(t) \tag{56}$$

where, once again, J is the constant diagonal matrix of Poincare exponents. Equation (56) can be expanded to

$$\begin{bmatrix} \dot{\eta}_1(t) \\ \dot{\eta}_2(t) \\ \vdots \\ \dot{\eta}_n(t) \end{bmatrix} = \begin{bmatrix} \lambda_1\eta_1(t) \\ \lambda_2\eta_2(t) \\ \vdots \\ \lambda_n\eta_n(t) \end{bmatrix} + \Lambda^{-1}(t)B(t)\bar{u}(t) \tag{57}$$

Since the system allowed diagonalization, which in this case can also be viewed as modal separation, it became obvious that feeding back a portion of the single unstable mode was possible. More importantly, the diagonalization provided for a relatively easy implementation of the control.

Control Law and Gain Calculation

As stated in Chapter III, the Poincare exponent analysis produced two stable modes and one unstable planar mode. Since all attracting bodies (earth, moon, sun) were initially assumed to lie in a plane, no forces which would cause out-of-plane satellite motions were present. Therefore, the derivation of the controller was based on the planar modes only, i.e. the state vector for controller design was $[R_x \; p_x \; R_y \; p_y]^T$. Since the controller could not realistically produce instantaneous position changes, the controller was physically constrained to create inertial velocity changes only. The difficulty encountered by Smith in his work, coupled with the preceding physical constraint, led to the choice of the simplest possible B matrix. The chosen B matrix was $[0 \; 1 \; 0 \; 1]^T$. Again, since in the chosen coordinate frame the momenta are inertial velocities, this choice for B was possible. The modal equations, then, were

$$\begin{bmatrix} \dot{\eta}_1(t) \\ \dot{\eta}_2(t) \\ \dot{\eta}_3(t) \\ \dot{\eta}_4(t) \end{bmatrix} = \begin{bmatrix} \lambda_1 & & & \\ & \lambda_2 & & [0] \\ & & \lambda_3 & \\ & [0] & & \lambda_4 \end{bmatrix} \begin{bmatrix} \eta_1(t) \\ \eta_2(t) \\ \eta_3(t) \\ \eta_4(t) \end{bmatrix} + \Lambda^{-1} \begin{bmatrix} 0 \\ 1 \\ 0 \\ 1 \end{bmatrix} u \quad (58)$$

where u is the scalar control, also chosen for simplicity. Choosing a scalar control and a B matrix as defined above is equivalent to assuming that the control is applied to the satellite at 45° angles from the rotating +x and +y axes shown in Figure 3 (since p_x and p_y receive equal amounts of control). Defining η_3 as the unstable component of the modal vector, the control law became

$$u = k\eta_3 \quad (59)$$

where k is the constant control gain. Recalling the definition of the modal variables, (50), the control law in physical variables was

$$u = k\bar{\Lambda_3^{-1}}(t)\delta\bar{x}(t) \quad (60)$$

where $\bar{\Lambda_3^{-1}}(t)$ is defined as the third row of $\Lambda^{-1}(t)$.

To calculate a value for k which will theoretically stabilize the linearized system, (49), requires a solution of the unstable component of (58).

$$\dot{\eta}_3(t) = \lambda_3\eta_3(t) + [\bar{\Lambda_{3\,2}^{-1}}(t) + \bar{\Lambda_{3\,4}^{-1}}(t)]k\eta_3(t) \quad (61)$$

($\eta_3(t)$ and $\eta_4(t)$ were defined as the unstable, planar mode, while $\eta_1(t)$ and $\eta_2(t)$ constituted the stable, planar mode.) The terms $\bar{\Lambda_{3\,2}^{-1}}(t)$ and $\bar{\Lambda_{3\,4}^{-1}}(t)$ were a result of multiplying

$\Lambda_3^{-1}(t)$ by the B vector (the 32 subscript denotes third row, second column). Rearranging (61) yields

$$\dot{\eta}_3(t) = \{\lambda_3 + [\lambda_{32}^{-1}(t) + \lambda_{34}^{-1}(t)]k\}\eta_3(t) \tag{62}$$

a linear, first order, time-varying differential equation for $\eta_3(t)$. The above equation can be solved via the method of an integrating factor. For notational simplicity, define

$$\gamma(t) = \Lambda_{32}^{-1}(t) + \Lambda_{34}^{-1}(t) \tag{63}$$

By the method of an integrating factor

$$\{e^{-\int[\lambda_3+k\gamma(t)]dt}\}\dot{\eta}_3(t) = [\lambda_3+k\gamma(t)]\{e^{-\int[\lambda_3+k\gamma(t)]dt}\}\eta_3(t) \tag{64}$$

From the Fourier analysis of Λ^{-1} (described in the next section), it was discovered that $\Lambda_{32}^{-1}(t)$ and $\Lambda_{34}^{-1}(t)$ had both constant and periodic components; therefore, $\gamma(t)$ can be separated into a periodic function and a constant.

$$\gamma(t) = \gamma_o + \gamma_p(t) \tag{65}$$

where γ_o is the constant and $\gamma_p(t)$ is the periodic function. The integrating factor expands to

$$e^{-\int[\lambda_3 + k\gamma_o + k\gamma_p(t)]dt} \tag{66}$$

which simplifies to

$$[e^{-(\lambda_3 + k\gamma_o)t}][e^{-\int k\gamma_p(t)dt}] \tag{67}$$

Making the above substitution and realizing that the multiplication by the integrating factor produces a perfect differential, one can write the differential

$$\frac{d}{dt}\{\eta_3(t)[e^{-(\lambda_3 + k\gamma_o)t}][e^{-\int k\gamma_p(t)dt}]\} = 0 \qquad (68)$$

and the solution to the above equation is

$$\eta_3(t) = c[e^{\int k\gamma_p(t)dt}][e^{(\lambda_3 + k\gamma_o)t}] \qquad (69)$$

where c is the constant of integration. The stability information, then, is contained in the last exponential of (69), since the periodic term will merely contribute oscillatory motion to the system. The shift in the root of η_3, then, will be governed by

$$\lambda_3' = \lambda_3 + k\gamma_o \qquad (70)$$

where λ_3' is defined as the new root location after control is applied.

Implementation of the Controller

The final implementation of the controller was accomplished by integrating the full non-linear equations of motion, described by (12) and augmenting the equations with the controller described in (60). Since the controller was designed for the linearized system, no assurance of a stabilizing system existed when the augmented non-linear equations were integrated. The vector $\delta\bar{x}(t)$ was formed by evaluating the state of the non-linear equations at time, t, and subtracting the state of the periodic reference

orbit at the same time, e.g.

$$\delta\bar{x}(t) = \bar{x}(t) - \bar{x}_{ref}(t) \tag{71}$$

The matrix, $\Lambda^{-1}(t)$, required by the control law, (60), was produced as follows. The eigenvectors of the system were computed by integrating (48) with a small, constant integration step. A Fourier series was then constructed to represent the elements of the eigenvectors at each integration step such that, given the time, one could produce the eigenvectors for the system at any point along the orbit from the Fourier series (Ref 2:60). Since $\Lambda(t)$ was composed of the system eigenvectors in accordance with (44), the $\Lambda(t)$ matrix was then produced from the Fourier series and its inverse computed at many points evenly spaced along the orbit. The components of the $\Lambda^{-1}(t)$ matrix were then Fourier analyzed to allow the $\Lambda^{-1}(t)$ matrix to be constructed at any given time.

V. Results, Conclusions, and Recommendations

Calculation of Controller Gain

Smith, in his work, derived a method for plotting what he termed a "quasi root locus" for a variational system forequations with periodic coefficients (Ref. 8:29). If the coefficient matrix, A(t) (also called the plant matrix in control literature), was a constant matrix, conventional root locus techniques could be employed to determine the shift in system roots as control gain is varied. In the system described by (49), however, the matrix A(t), is time periodic; therefore, a conventional root locus plot of gain versus frequency is not possible. Equation (49) though, can also be solved by Floquet theory. Smith realized that since Poincare exponents are determinants of system stability in a Floquet analysis, solving the augmented state equations for the Poincare exponents for various values of gain results in a "quasi root locus". Implementing Smith's theory enabled the calculations required to plot the root locus for the system with modal control, and the plot is shown in Figure 5. As predicted by the modal control theory of Chapter IV, the unstable root migrated to the left on the real axis and became more negative as gain was increased. Since none of the other system roots were affected, it is obvious why modal control can be

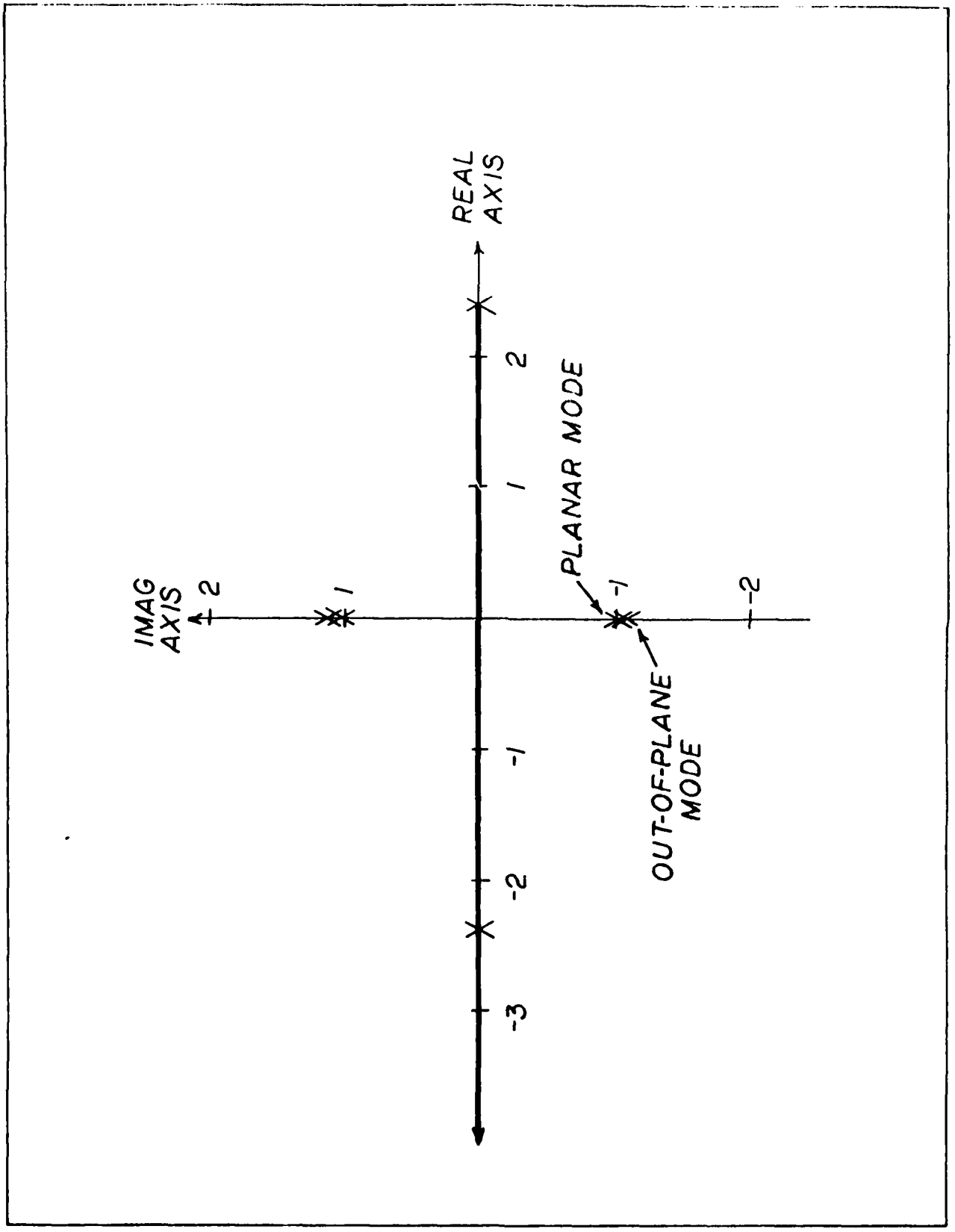

Figure 5. Quasi Root Locus

viewed as a pole placement technique. The values of gain used were k = 0.0, 0.259, 0.359, 0.459, 0.559, and 1.0. As calculated from (70), the minimum gain to stabilize the system was, in fact, k = 0.259. The root locus analysis also enables one to plot the unstable exponent, λ_3, versus control gain, and this plot is shown in Figure 6. The linear relationship between frequency and gain was unpredicted, but was later explained by the gain calculation of (70). Since the constant portions of $\Lambda_{32}^{-1}(t)$ and $\Lambda_{16}^{-1}(t)$ were found to be -0.9857 and -8.256, respectively, the predicted slope of the λ_3 vs. gain plot of Figure 6 was 9.2417. The actual slope of Figure 6 was, in fact, 9.2414, thus verifying the validity of Equation (70).

Evaluation of the Controller

As stated in Chapter IV of this report, the controller design was based on a linearized set of equations and yet the controller was incorporated into the non-linear equations of motion. This evaluation technique was implemented to test the controller in the most realistic model (available to this study) of the actual dynamics of the system. Care was exercised in the choice of initial conditions to insure that the system was initially inside the region where the linearization was valid.

Recalling the form of the modal variables,

$$\bar{\eta}(t) = \Lambda^{-1}(t)\delta\bar{x}(t) \qquad (72)$$

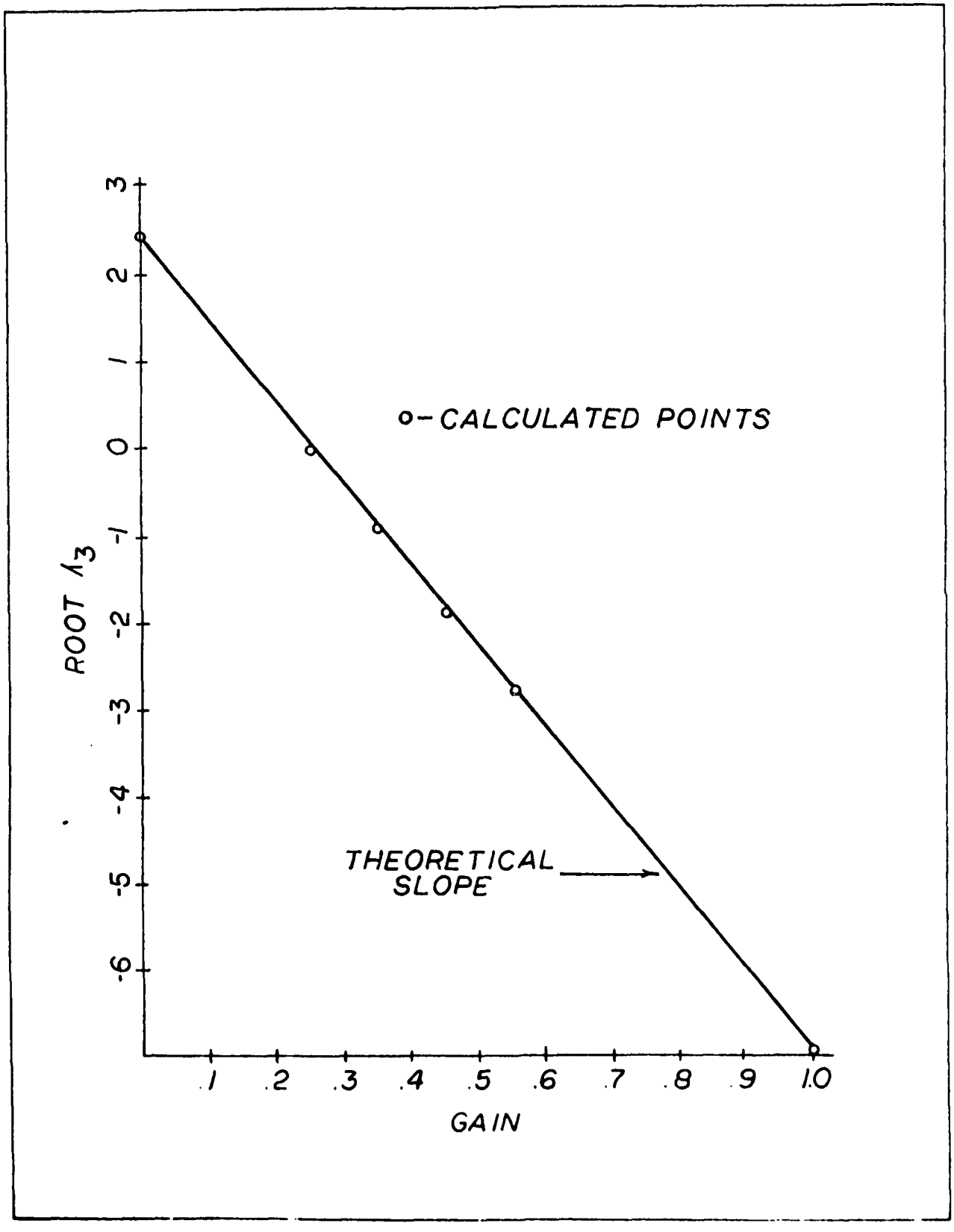

Figure 6. λ_3 vs Gain

The ideal controller should drive the modal variables to zero, since one desires

$$\delta\bar{x}(t) = \bar{x}(t) - \bar{x}_{ref}(t) = \bar{0} \tag{73}$$

However, since only η_3 was controlled, one would anticipate the stable planar mode, η_1, and η_2, would oscillate (due to purely complex roots) while the negative real portion of the unstable mode, η_4, exponentially decreases. In the absence of control, η_3 should exponentially increase. These concepts are mathematically demonstrated by recalling (58) from Chapter IV of this report. If u = 0 (no control), (58) reduces to

$$\dot{\bar{\eta}}(t) = \begin{bmatrix} \lambda_1 & & & \\ & \lambda_2 & & [0] \\ & & \lambda_3 & \\ [0] & & & \lambda_4 \end{bmatrix} \bar{\eta}(t) \tag{74}$$

which is a constant coefficient set of equations. Since λ_1 and λ_2 are purely complex conjugates and λ_3 and λ_4 are a real conjugate pair, the theoretical solution to (74) is of the form

$$\begin{bmatrix} \eta_1(t) \\ \eta_2(t) \\ \eta_3(t) \\ \eta_4(t) \end{bmatrix} = \begin{bmatrix} \eta_{10}\cos(\lambda_1 t) + \eta_{20}\sin(\lambda_1 t) \\ \eta_{20}\cos(\lambda_1 t) - \eta_{10}\sin(\lambda_1 t) \\ \eta_{30}e^{\lambda_3 t} \\ \eta_{40}e^{-\lambda_3 t} \end{bmatrix} \tag{75}$$

where η_{10}, η_{20}, η_{30}, and η_{40} are the initial conditions defined by (72) at t = 0. Figures 7 and 8 are plots of theoretical and computed magnitudes of the modal variables for two orbital periods when no control is present (i.e. k = 0.0). The initial conditions (deviations from the reference periodic orbit), $\delta\bar{x}(0)$, were arbitrarily chosen to be -1.496 km in x and y position and -0.00298 cm/sec in x and y momenta. Recalling the orbital period was 0.508 in the units of Chapter II. Figure 7 and 8 plot two orbits (two months). As shown by the two figures, the computed solutions track the theoretical solutions quite well.

When the control was applied, the same behavior was seen in the uncontrolled mode, as expected, but the controlled mode was forced to an approximately exponential decay. Figures 9 and 10 are plots of the modes with the controller activated. The plots cover four orbits about L3 and the controller gain was k = 0.359. Initial conditions chosen for this case were -149.6 km in x and y position, and -2.978 cm/sec in x and y momenta. To demonstrate the effect of increasing the gain of the controller, Figures 11 and 12 show plots with identical initial displacements as those in Figures 9 and 10, but the controller gain was increased to K = 0.559.

The oscillations around a pure cosine or sine curve of η_1, and η_2, and the overshoot past the zero level of η_4, may both, in part, be attributed to the mathematical construction of the controller. The applied modal control

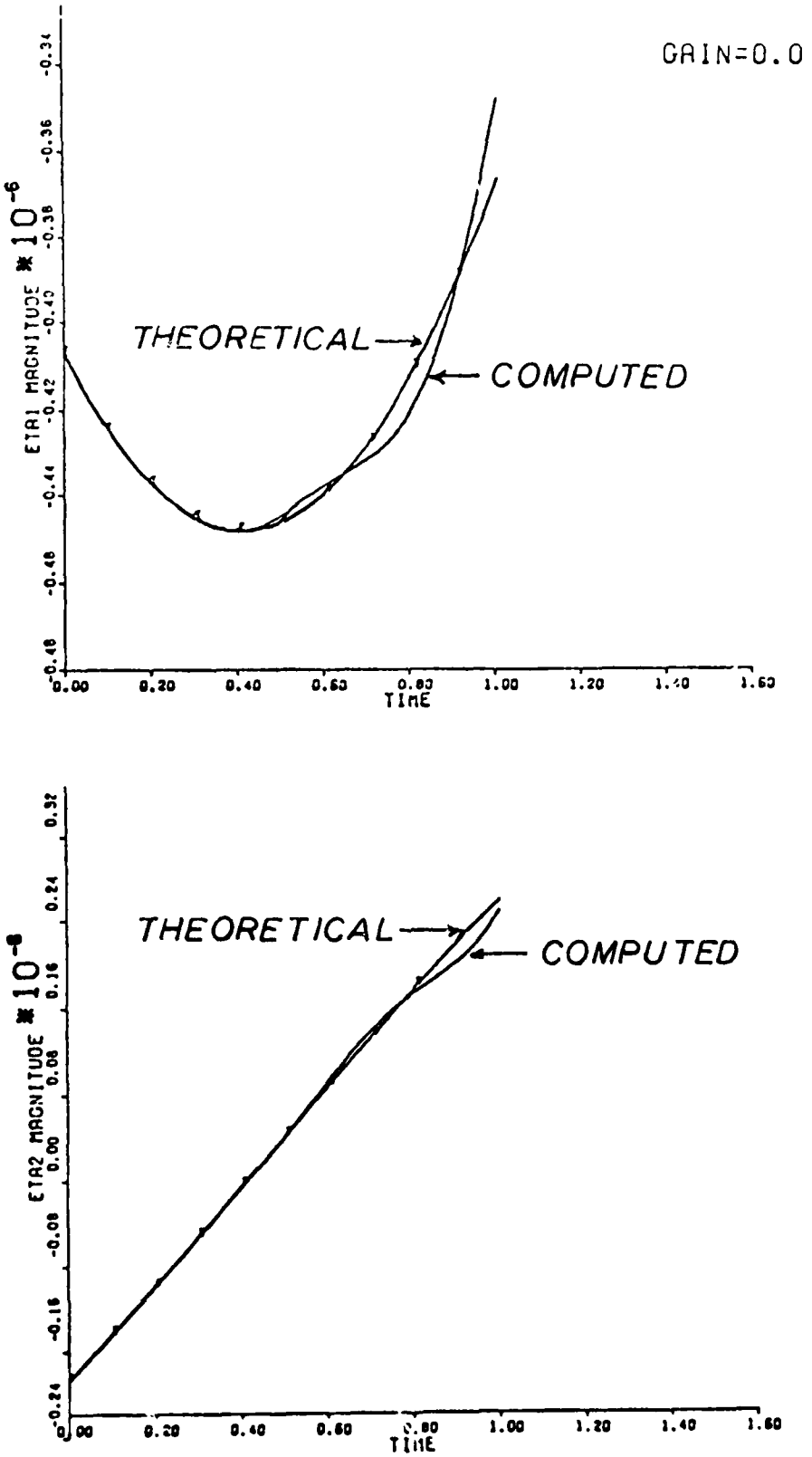

Figure 7. Theoretical and Computed Stable Mode (2 orbits)

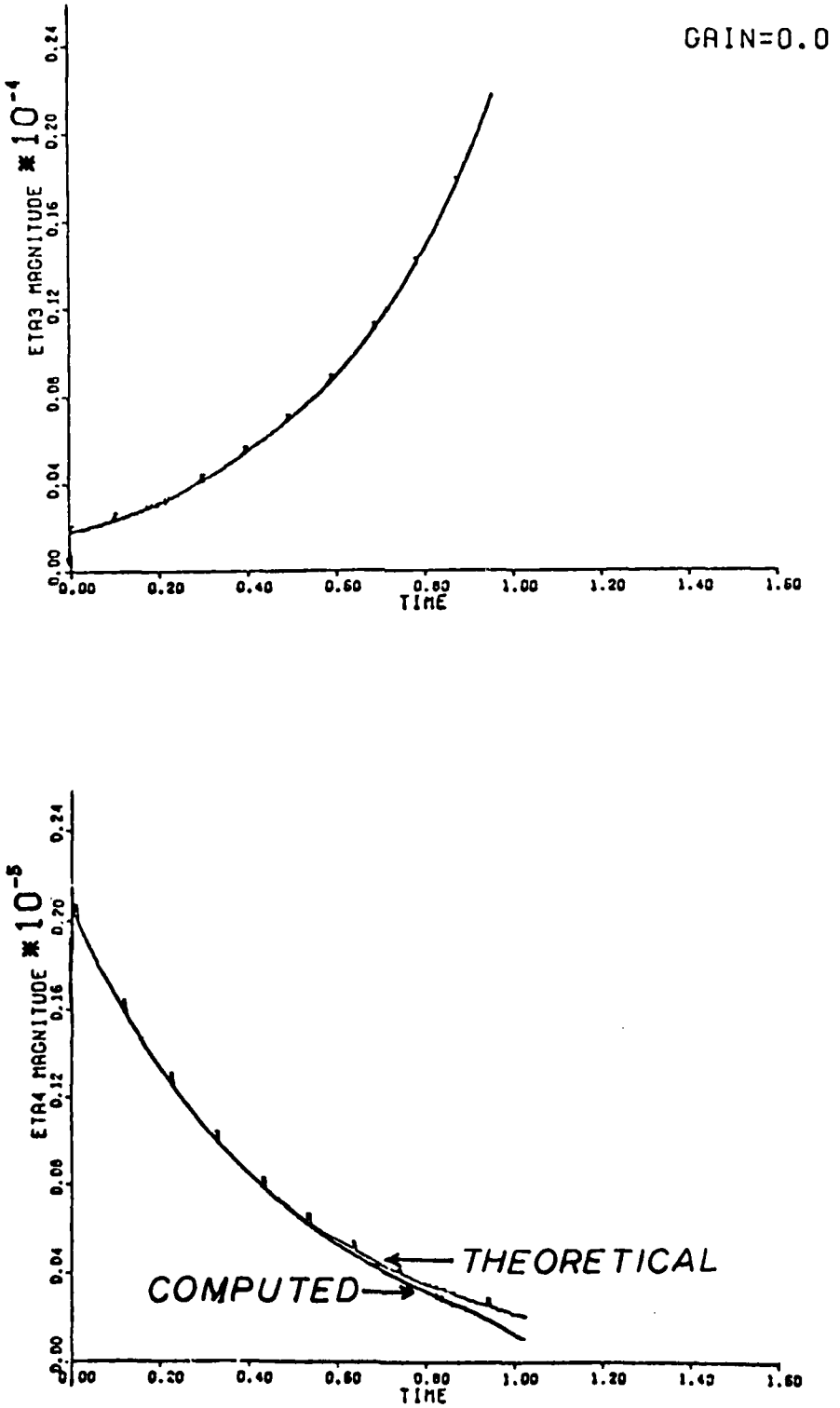

Figure 8. Theoretical and Computed Unstable Mode (2 orbits)

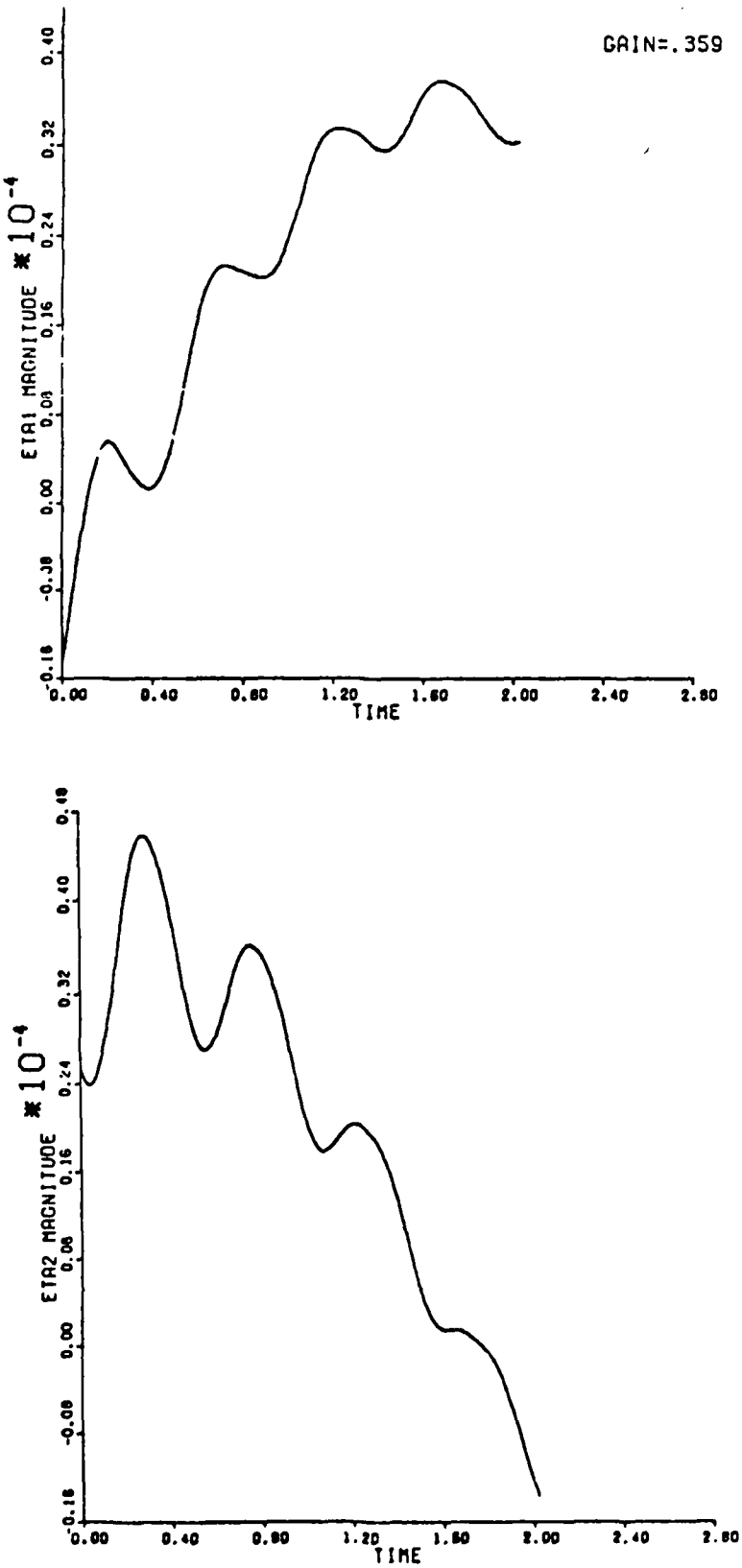

Figure 9. Stable Mode (4 orbits)

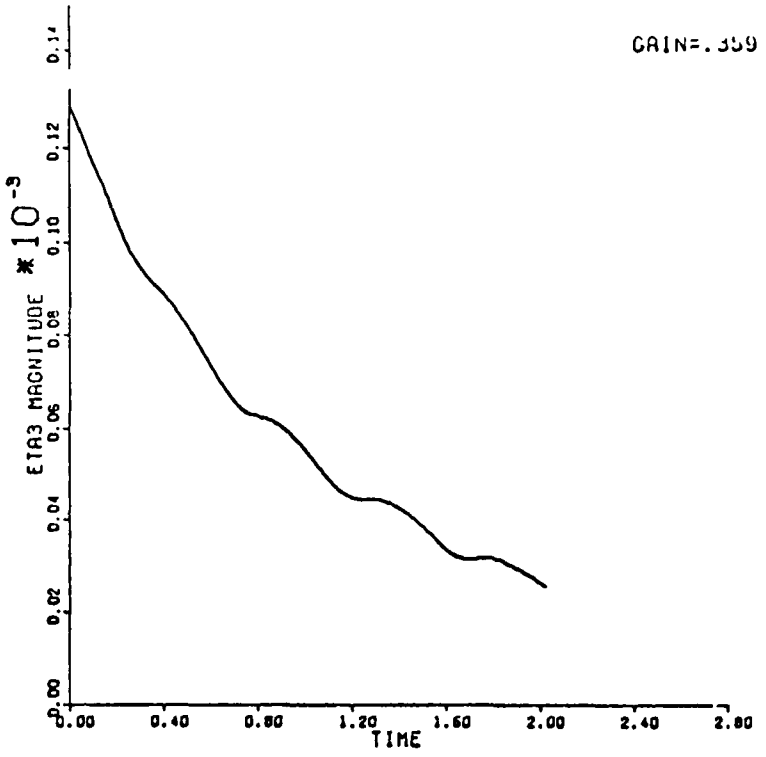

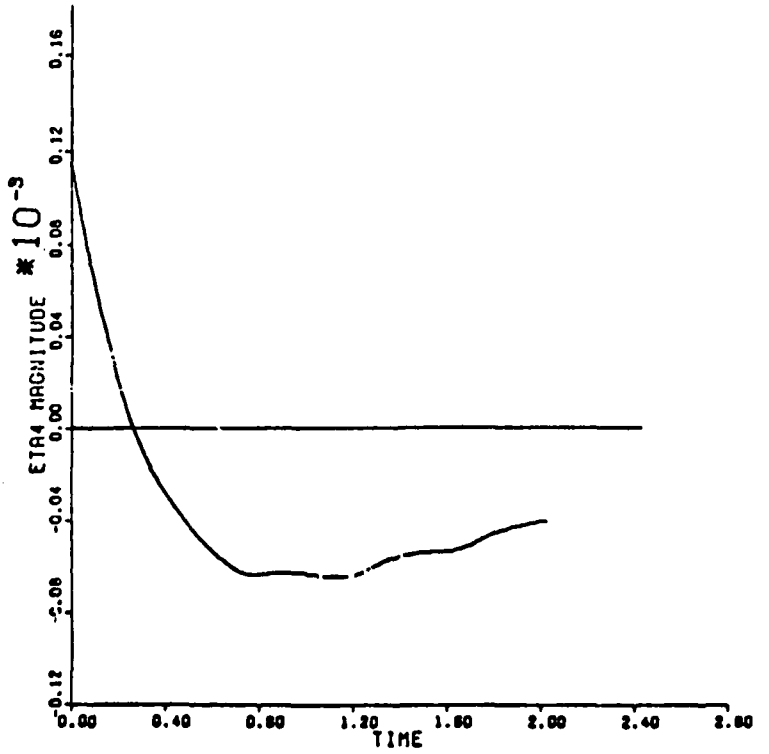

Figure 10. Unstable Mode (4 orbits)

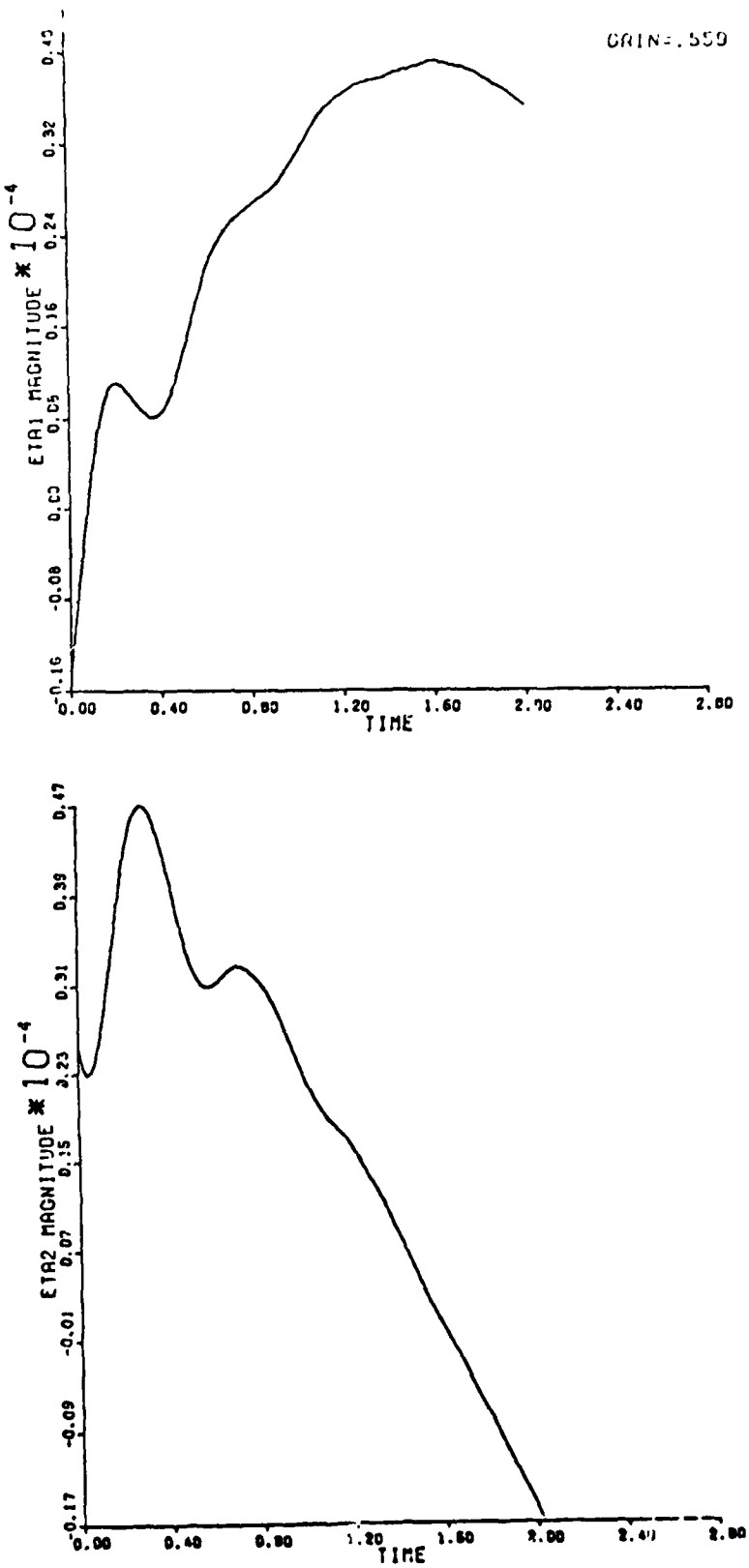

Figure 11. Stable Mode (4 orbits)

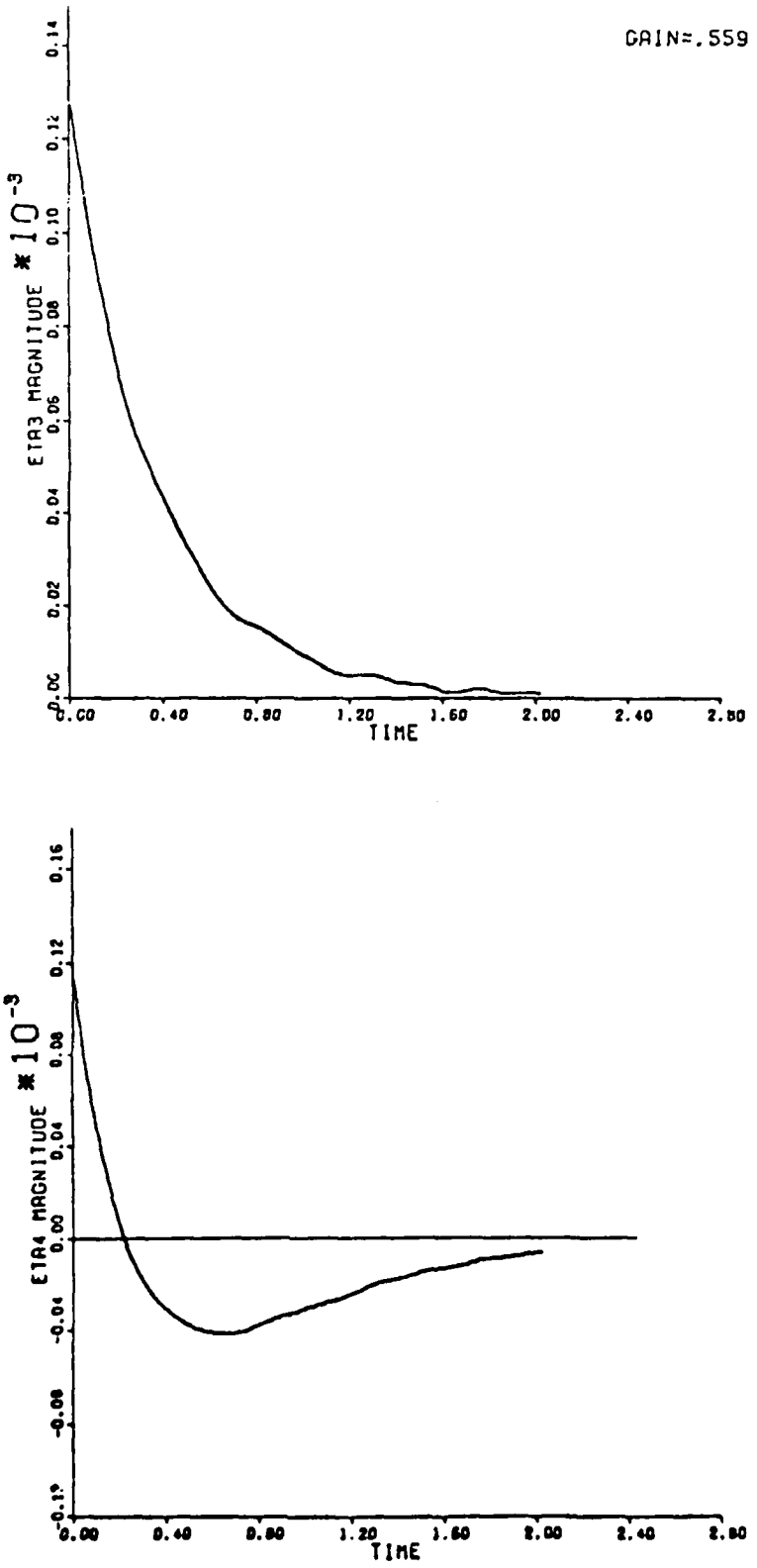

Figure 12. Unstable Mode (4 orbits)

does, in fact, change only the λ_3 frequency as seen by the root locus of Figure 5. Subsequent analysis illustrates that all system eigenvectors change, and this change in the eigenvectors causes a deviation in the modal behavior. This deviation, however, is insignificant as long as the system is stabilized. Figures 9-12 do portray a stabilized system.

When longer periods of controller operation were attempted, undamped oscillations began to occur in all modes. Figures 13 and 14 portray such a case. The magnitudes of the initial conditions chosen for this case were much smaller than those of Figures 9-12 (-1.496 km in x position, +1.496 km in y position, +0.00298 cm/sec in x momentum and -0.02978 cm/sec in y momentum for this case), and the chosen gain was k = 0.359. Figures 13 and 14 represent two years, or 24 orbits, of operation. In Figure 14, the oscillations occur in both η_3 and η_4 and the oscillations appear to be sinusoidal with a linearly increasing magnitude. It is also noteworthy that the controller did overcome the initial displacements, but then started to oscillate after attaining the desired zero level for η_3 and η_4.

To isolate the cause of the oscillations, the same case was run (k = 0.359, 24 orbits), but the initial displacements were removed such that $\delta\bar{x}(0) = \bar{0}$. Figures 15 and 16 demonstrate that the oscillations were actually present, though small (note the scale), before they were apparent in Figures 13 and 14.

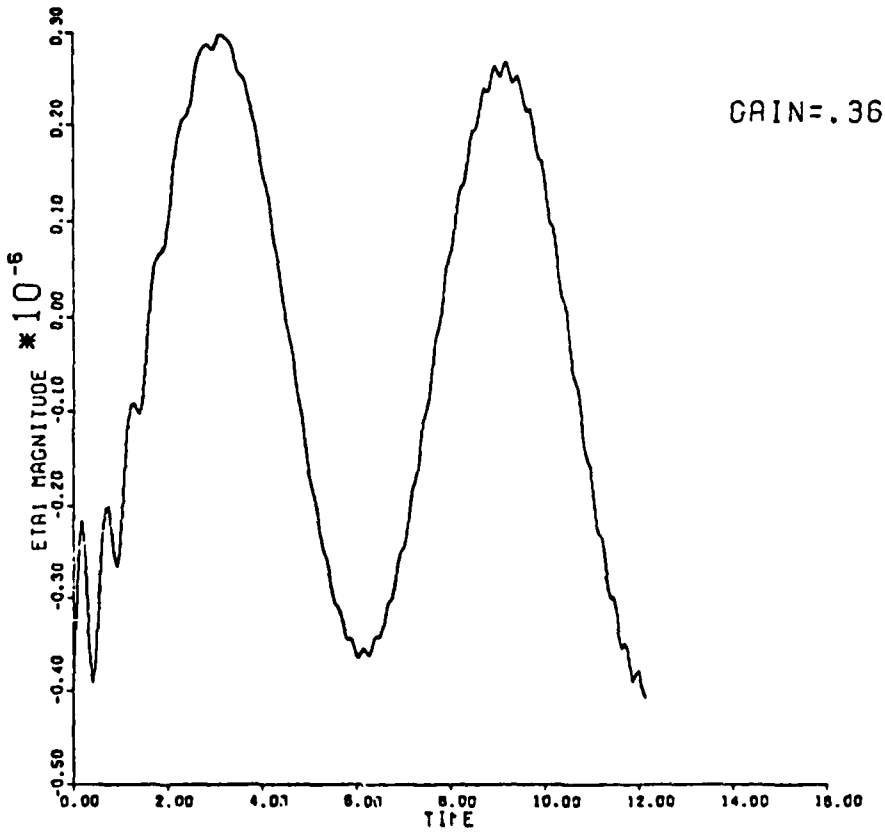

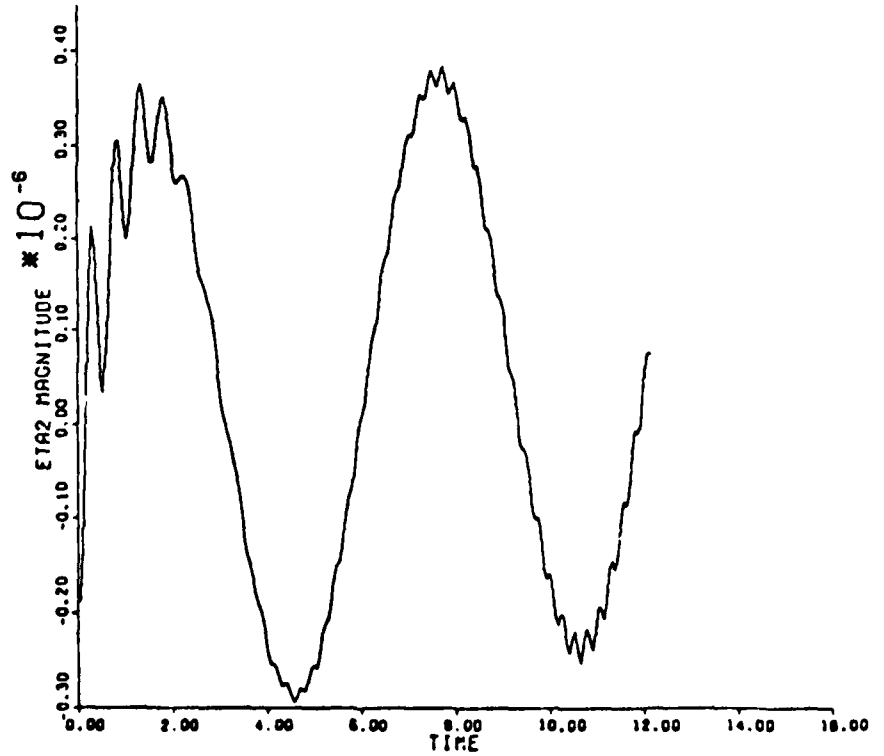

Figure 13. Stable Mode (24 orbits)

GAIN=.36

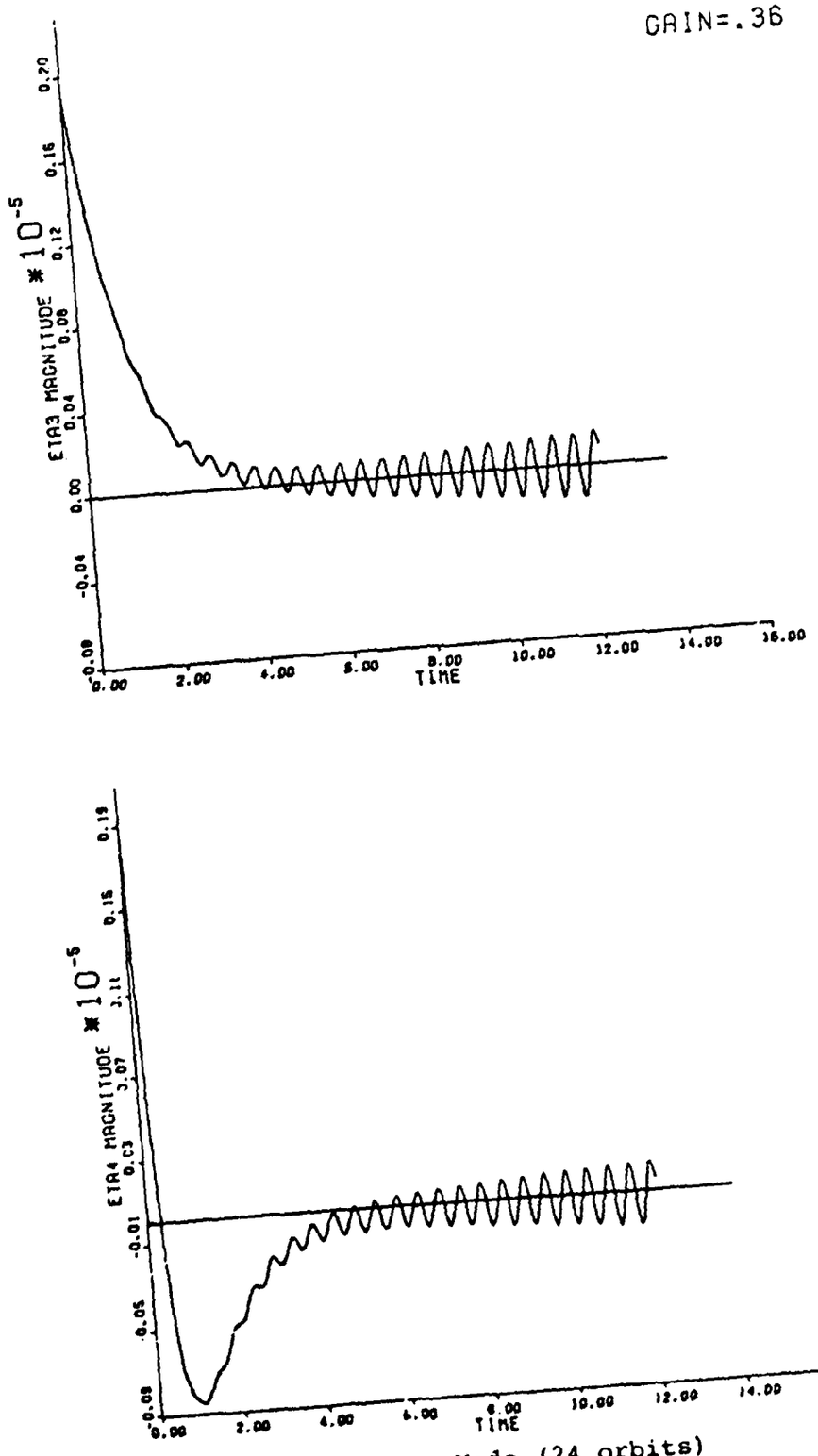

Figure 14. Unstable Mode (24 orbits)

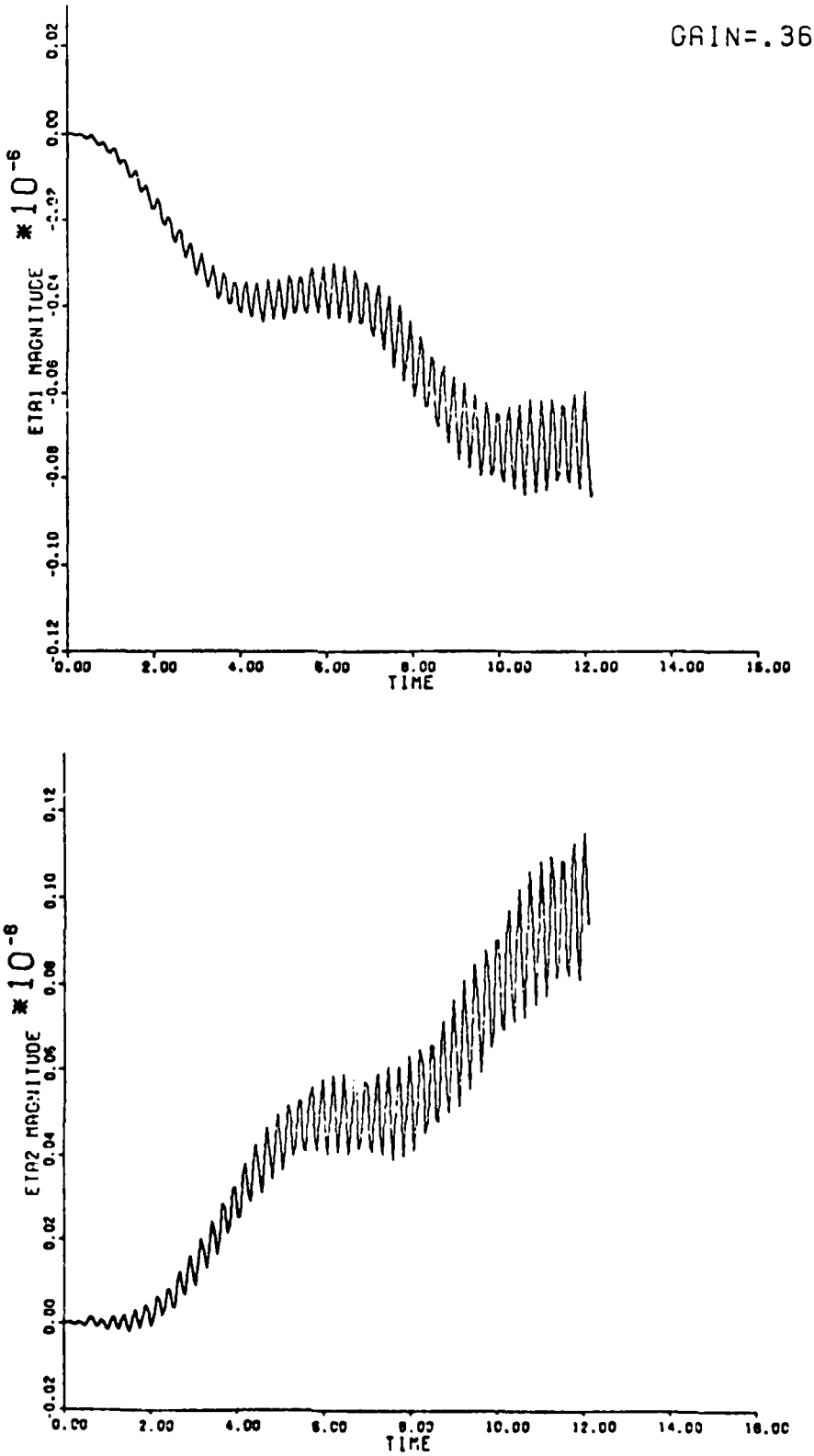

Figure 15. Stable Mode (24 orbits, $\delta\bar{x}(0) = \bar{0}$)

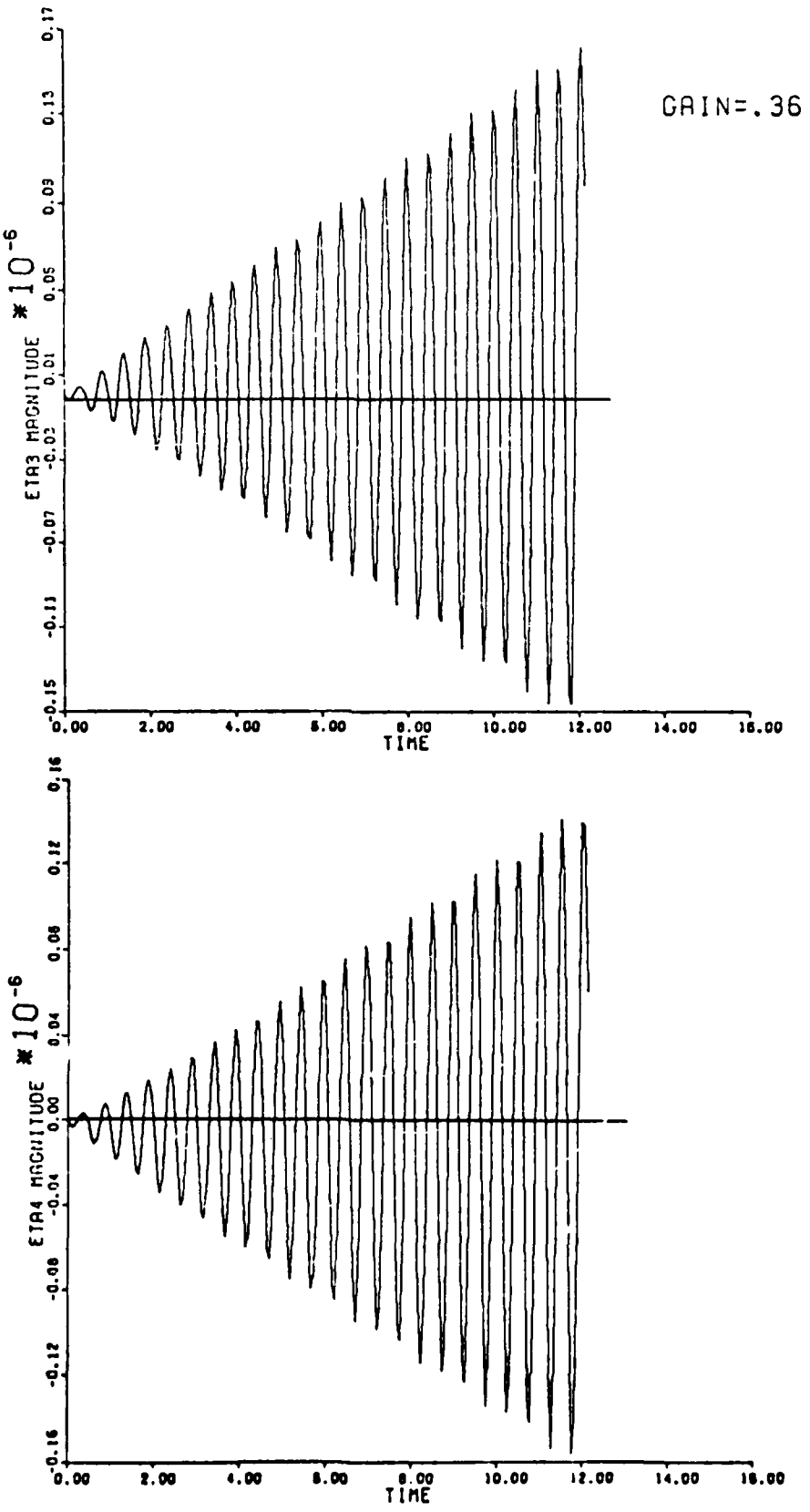

Figure 16. Unstable Mode (24 orbits, $\delta\bar{x}(0) = \bar{0}$)

Several possibilities were postulated for the oscillations seen in the results thus far. The first of these was an "out of sync" condition between the reference orbit of the satellite and the integrated non-linear equations of motion augmented with the controller. Since the L3 orbit is represented by a Fourier series, it is possible that the orbital frequency and the frequency of the integrated equations might become mismatched. To illustrate, assume that the integrated frequency, ω, is mismatched by a small factor, ε, such that the periodic motion is governed by a term such as

$$\sin(\omega t + \varepsilon t) \tag{76}$$

Expanding (76) yields

$$\sin(\omega t)\cos(\varepsilon t) + \cos(\omega t)\sin(\varepsilon t) \tag{77}$$

Since ε is small, $\cos(\varepsilon t) \cong 1$ and $\sin(\varepsilon t) \cong \varepsilon t$. Substituting these approximations into (77) yields

$$\sin(\omega t) + \cos(\omega t)\varepsilon t \tag{78}$$

which would produce the observed periodic motion plus an increasing amplitude term (mixed secular term). To investigate the possibility that the oscillations were a result of this frequency mismatch, the system was allowed to operate for one year (12 orbits) with no control. Figures 17 and 18 show this case which further demonstrates the behavior shown in Figures 7 and 8. Unlike Figures 7 and 8,

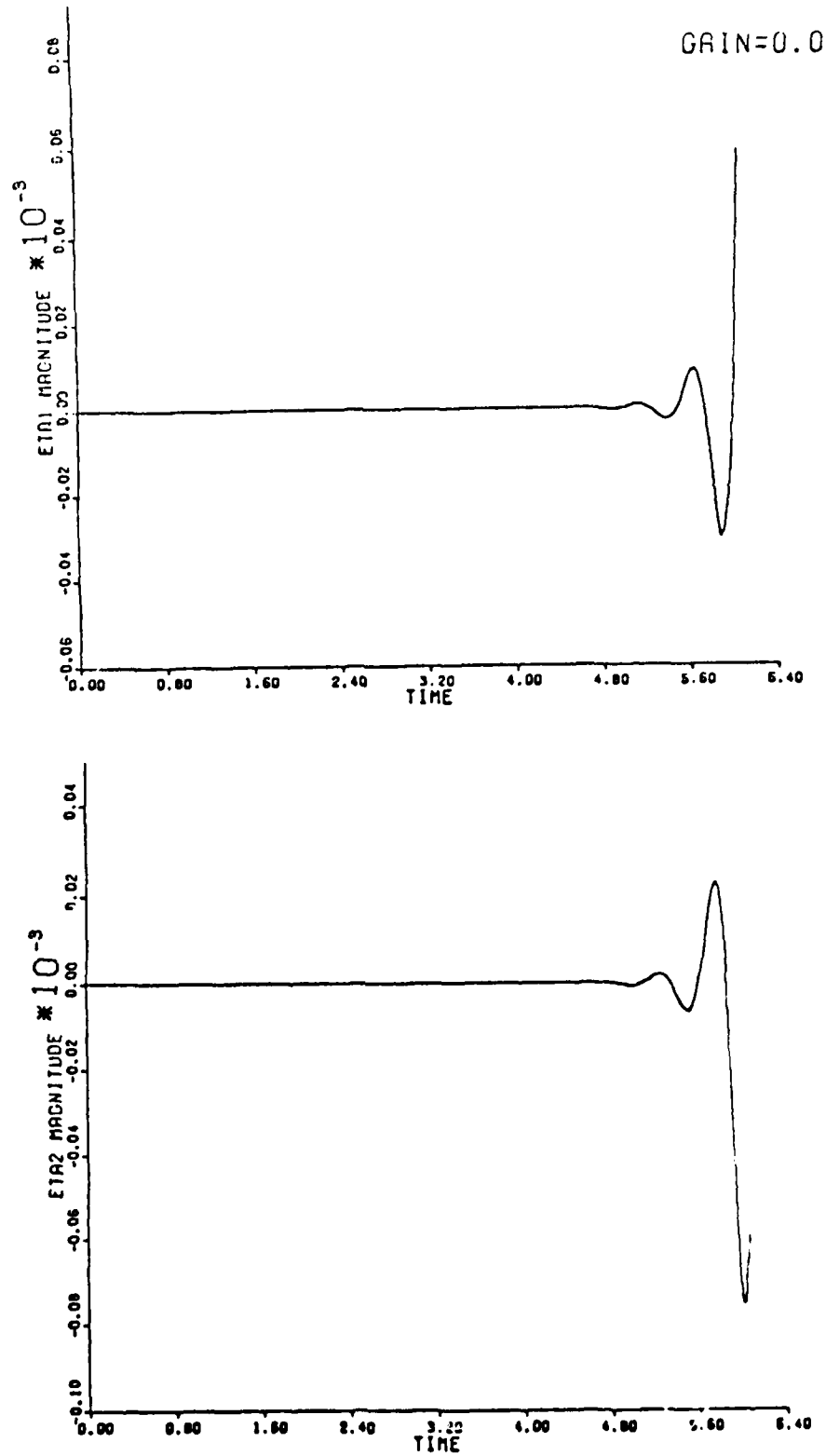

Figure 17. Stable Mode (12 orbits, $\delta\bar{x}(0) = \bar{0}$)

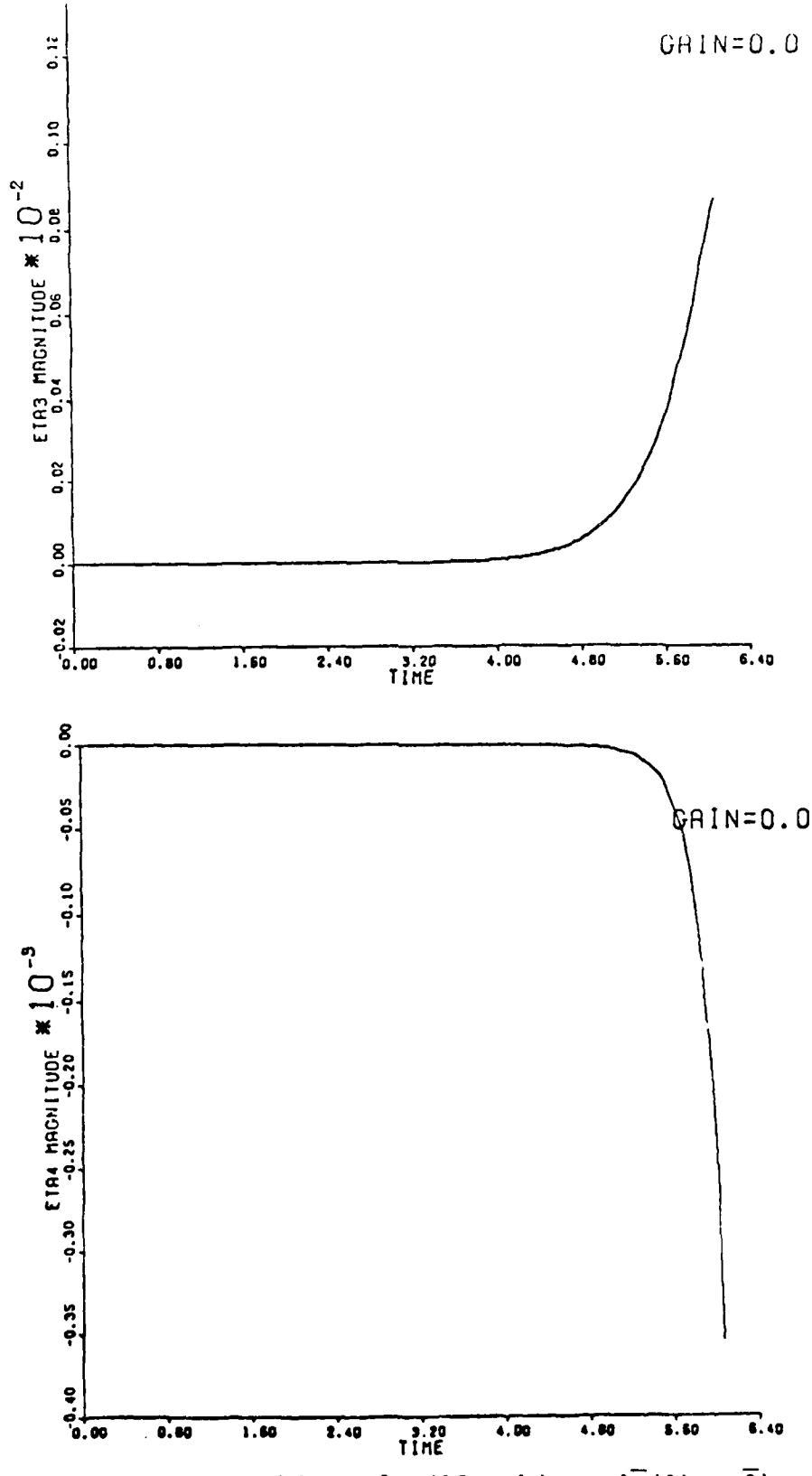

Figure 18. Unstable Mode (12 orbits, $\delta\bar{x}(0) = \bar{0}$)

however, Figures 17 and 18 represent a case with zero initial conditions. The modes, then, were well behaved for approximately seven months at which time the unstable eigenvalue, $e^{\lambda_3 t}$, had increased enough to dominate system behavior. Figures 19 and 20 further illustrate the need for control. After two years with no control, even though the initial conditions were zero, the system is totally out of the linear regime and the calculations were nonsensical.

Another possibility for the oscillations that merited investigation was the size of the integration step. If the step size were too large, the integration might be computing an inaccurate state vector, which then is used to calculate $\delta\bar{x}(t)$. When the step size was halved for the case shown in Figures 21 and 22, the oscillations remained. This case also had the controller inoperative and $\delta\bar{x}(0) = \bar{0}$.

Inclusion of Eccentricity and Inclination Effects

Chapter II of this report described the periodic orbit for the moon which was constructed by Wiesel. Results presented thus far are based on this lunar model. The Wiesel lunar orbit program, though, is also capable of providing the eccentricity and inclination effects of the moon. With these two forcing functions included in the lunar model, the controller was truly tested on a very realistic model of the earth-moon-sun system. With a control gain of 0.459 and the initial conditions set to zero, the system was operated for four months (4 orbits). Figures 23 and 24 depict the behavior of the modes for this case.

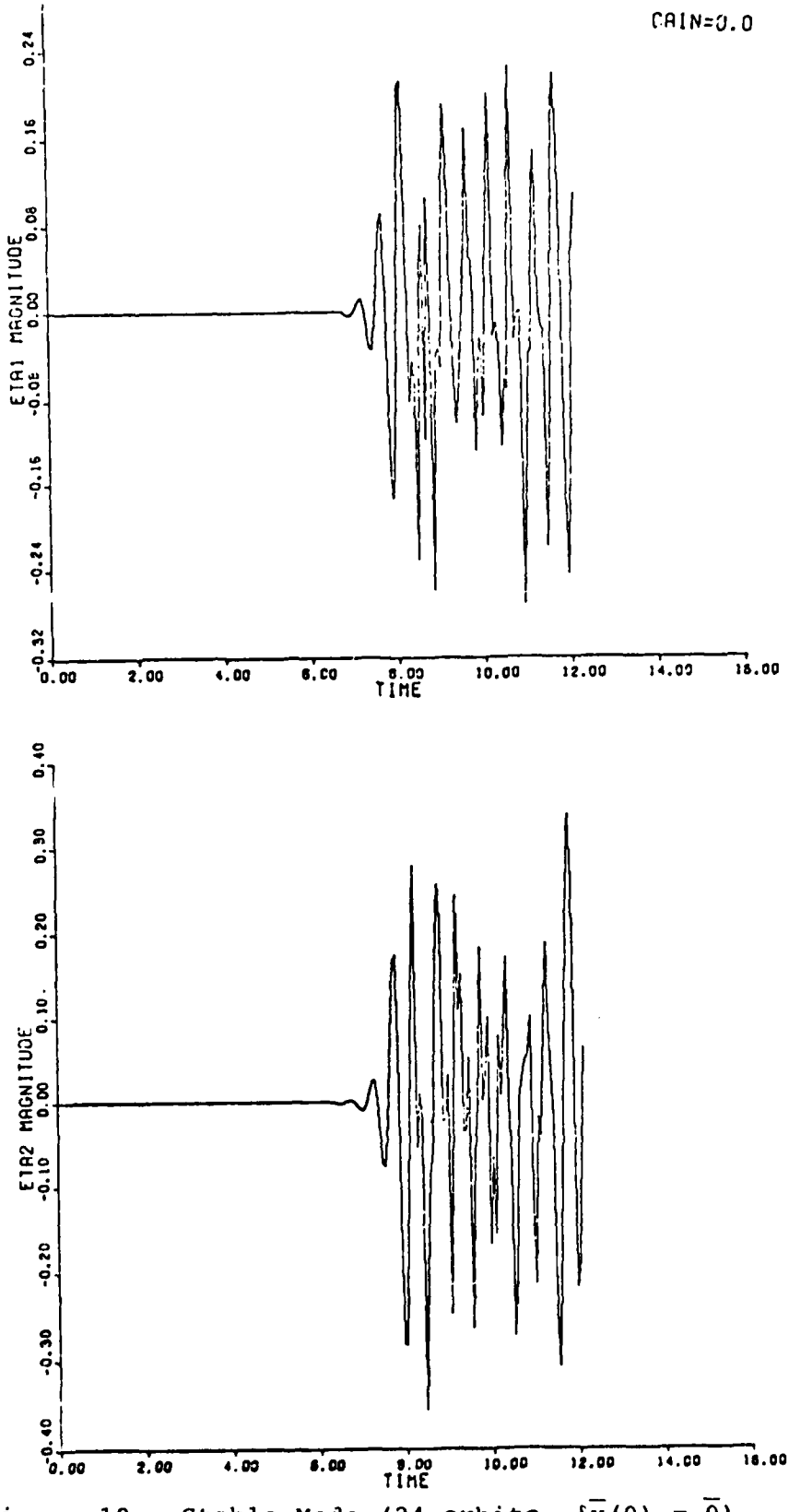

Figure 19. Stable Mode (24 orbits, $\delta\bar{x}(0) = \bar{0}$)

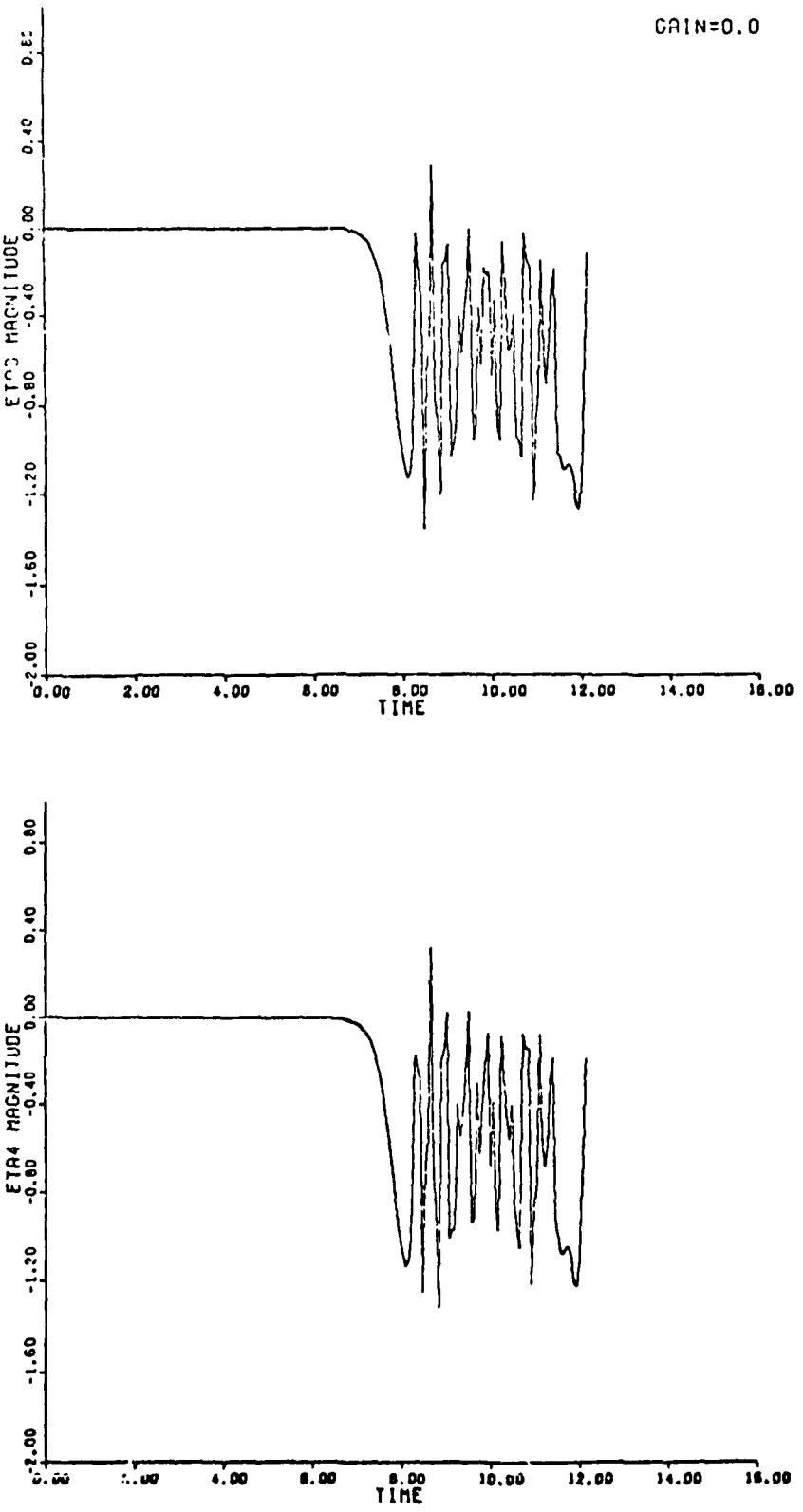

Figure 20. Unstable Mode (24 orbits, $\delta\bar{x}(0) = \bar{0}$)

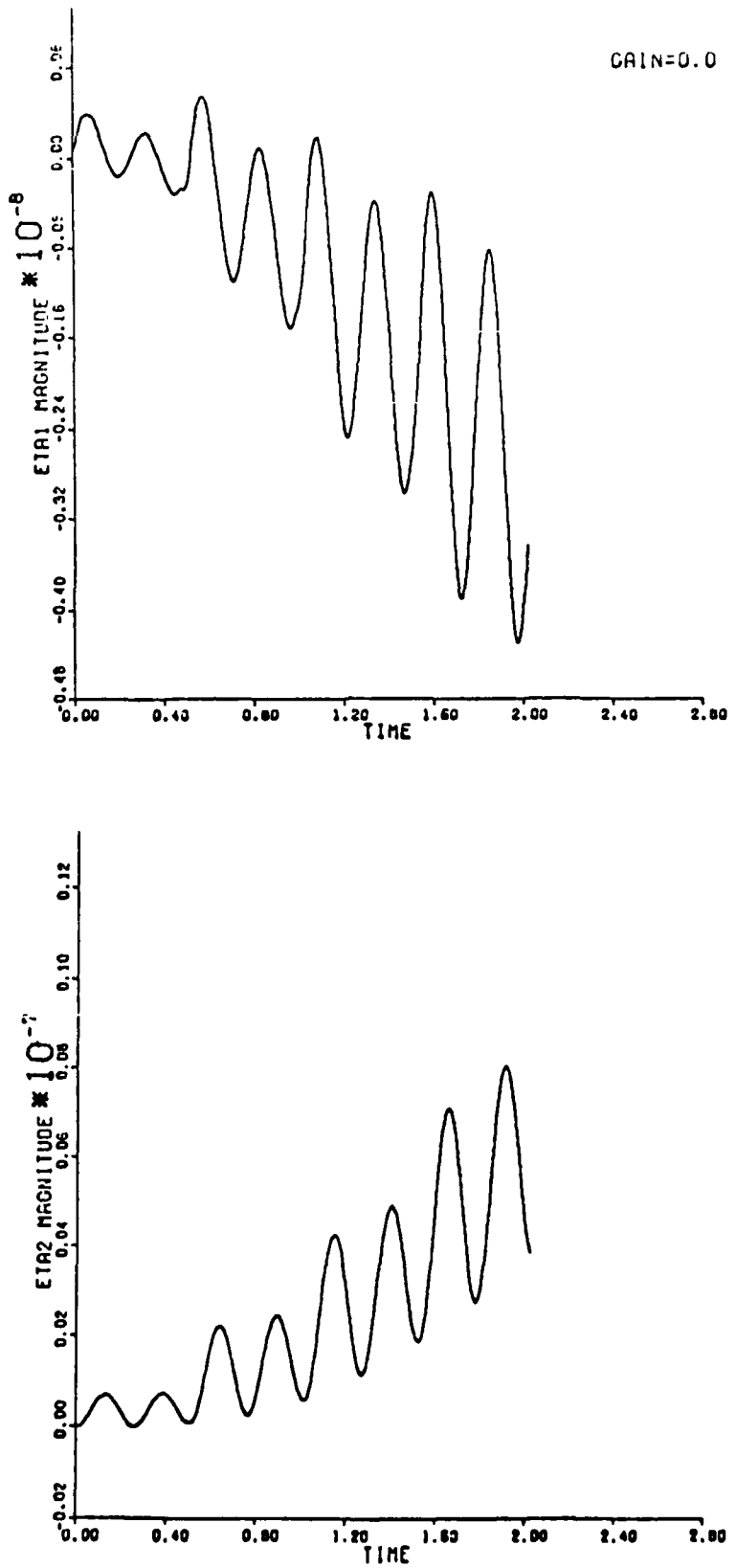

Figure 21. Stable Mode (4 orbits, $\delta\bar{x}(0) = \bar{0}$, smaller integration step size)

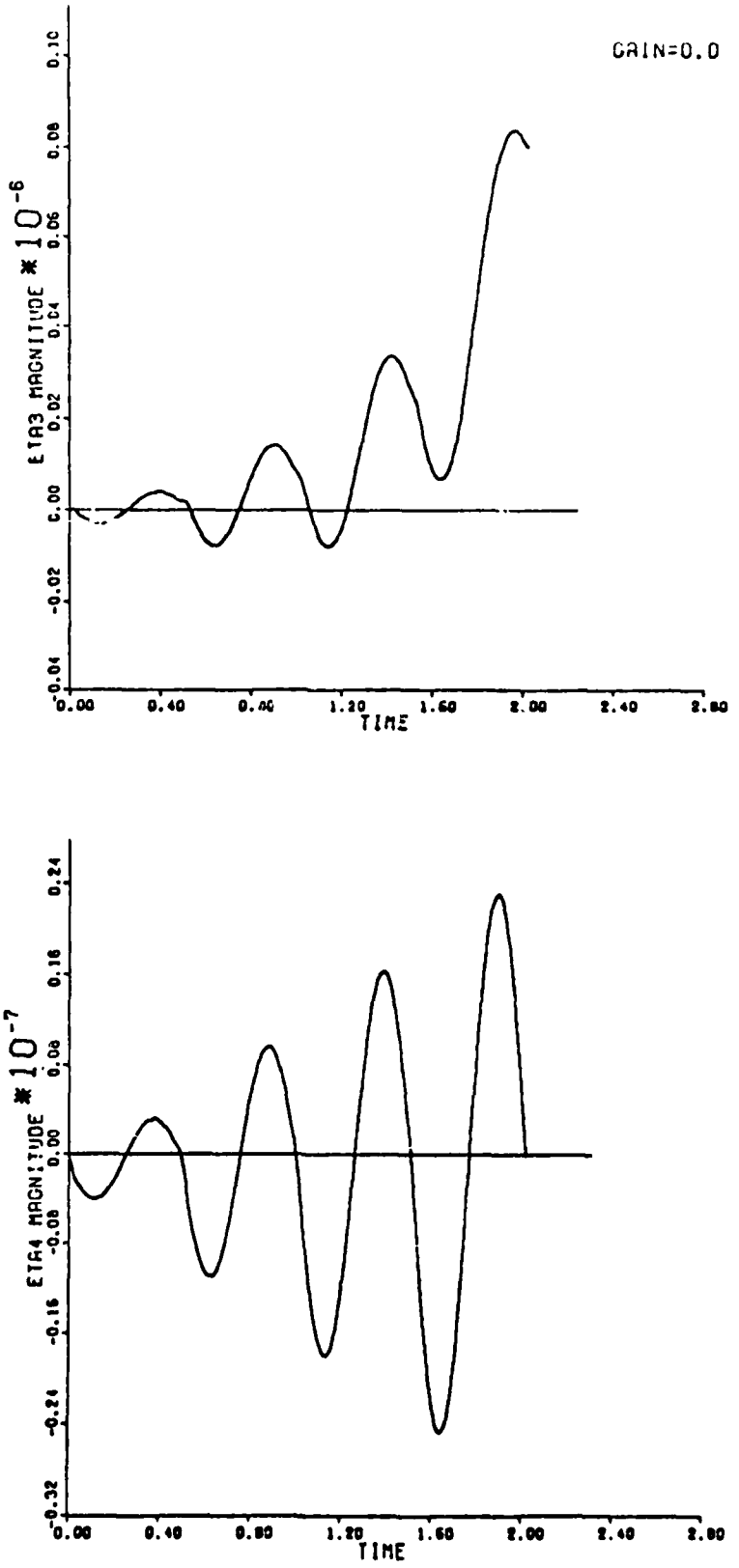

Figure 22. Unstable Mode (4 orbits, $\delta\bar{x}(0) = \bar{0}$, smaller integration step size)

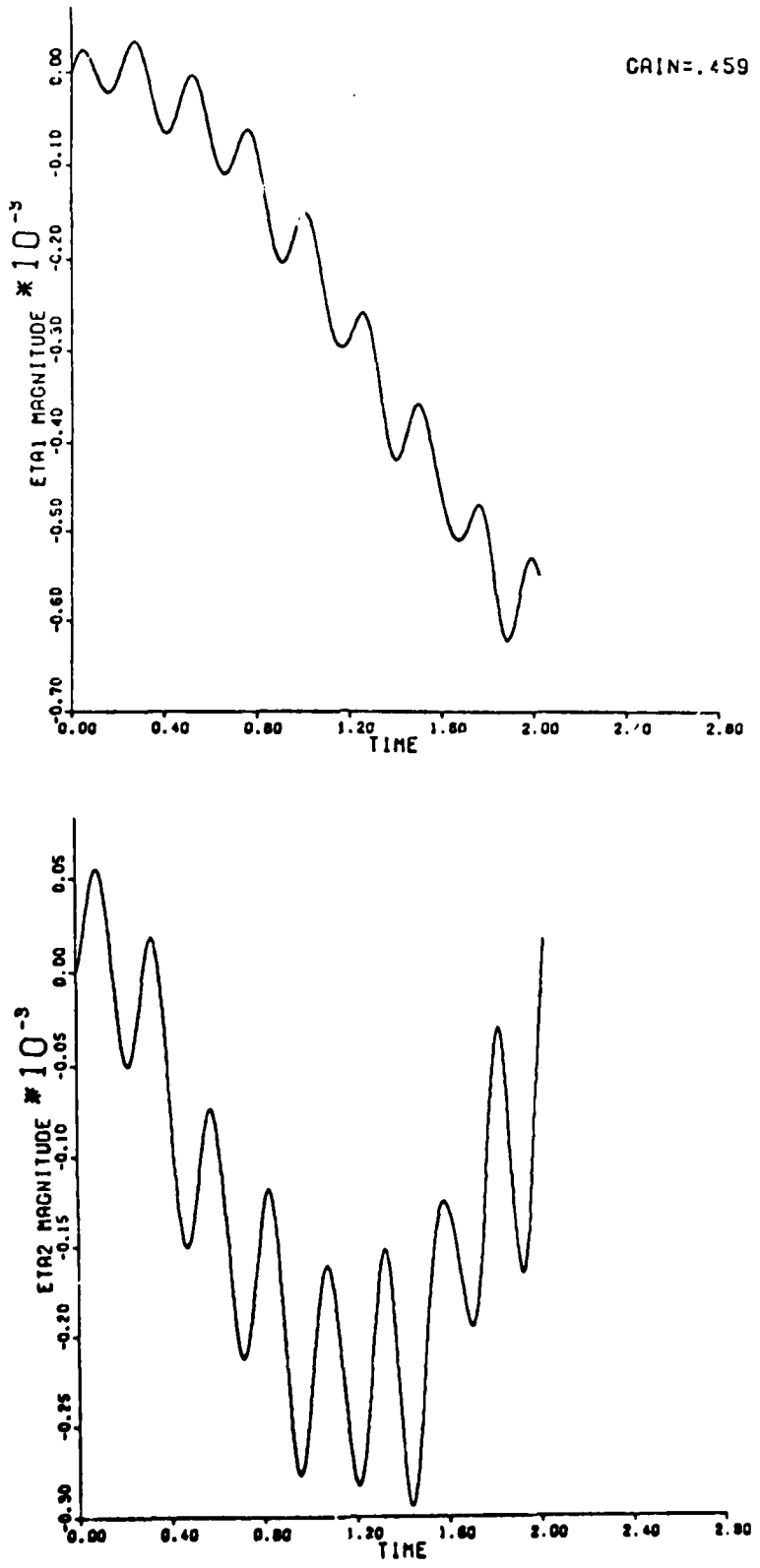

Figure 23. Stable Mode, Inclination and Eccentricity Effects Included (4 orbits, $\delta\bar{x}(0) = \bar{0}$)

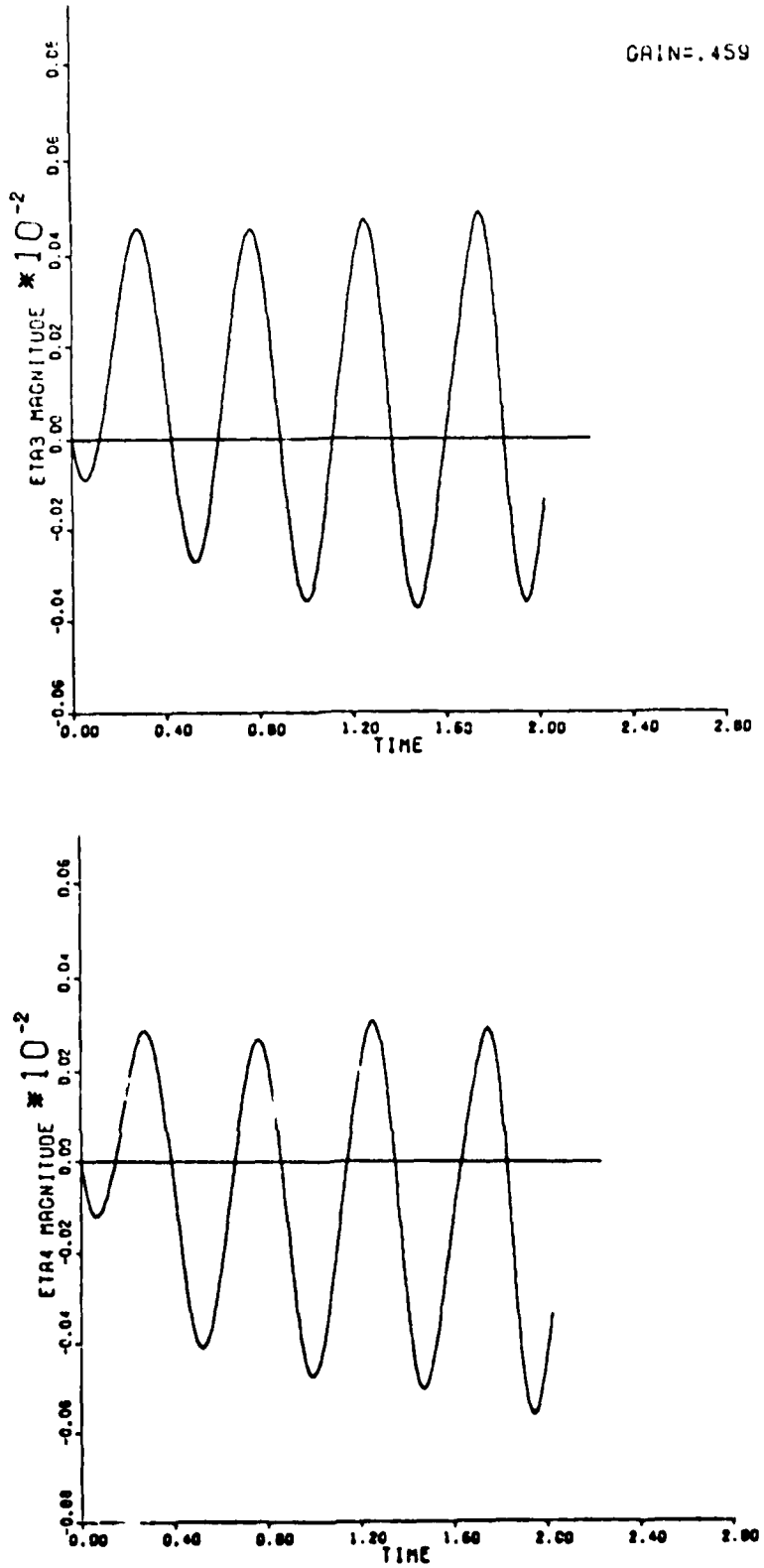

Figure 24. Unstable Mode, Lunar Inclination and Eccentricity Effects Included (4 orbits, $\delta\bar{x}(0) = \bar{0}$)

When Figures 23 and 24 are compared with Figures 15 and 16, one notices the oscillations are much larger in Figures 23 and 24, and the oscillations of η_3 and η_4 appear to have a frequency approximately equal to the orbital period.

The four components of $\delta\bar{x}(t)$ which are used to construct $\bar{\eta}$ are also plotted. Figure 25 portrays $\delta x_1(t)$ and $\delta x_2(t)$ while Figure 26 shows $\delta x_3(t)$ and $\delta x_4(t)$. The curves appear to reflect the same type of behavior demonstrated by the system prior to the inclusion of the forcing terms. The controller does maintain the $\delta\bar{x}(t)$ components around the zero level, but a periodic forcing term is readily apparent. For the four orbits, oscillations observed were approximately 4400 km in x position and 6000 km in y position.

Without the lunar inclination and eccentricity effects included, a calculated control cost is superfluous since it is not based on this study's most realistic model. Control costs were computed for the case described above which is shown in Figures 23-26. The control cost was computed by calculating the magnitude of the control applied. Since control is actually an acceleration (Δ velocity),

$$\Delta v = \int_0^t |\text{control acceleration}|\,dt \tag{79}$$

where Δv is the change in velocity. To compute an average control acceleration, then,

$$\bar{a} = \frac{1}{t}\int_0^t |\text{control acceleration}|\,dt \tag{80}$$

where $\bar{a}$ is the average acceleration.

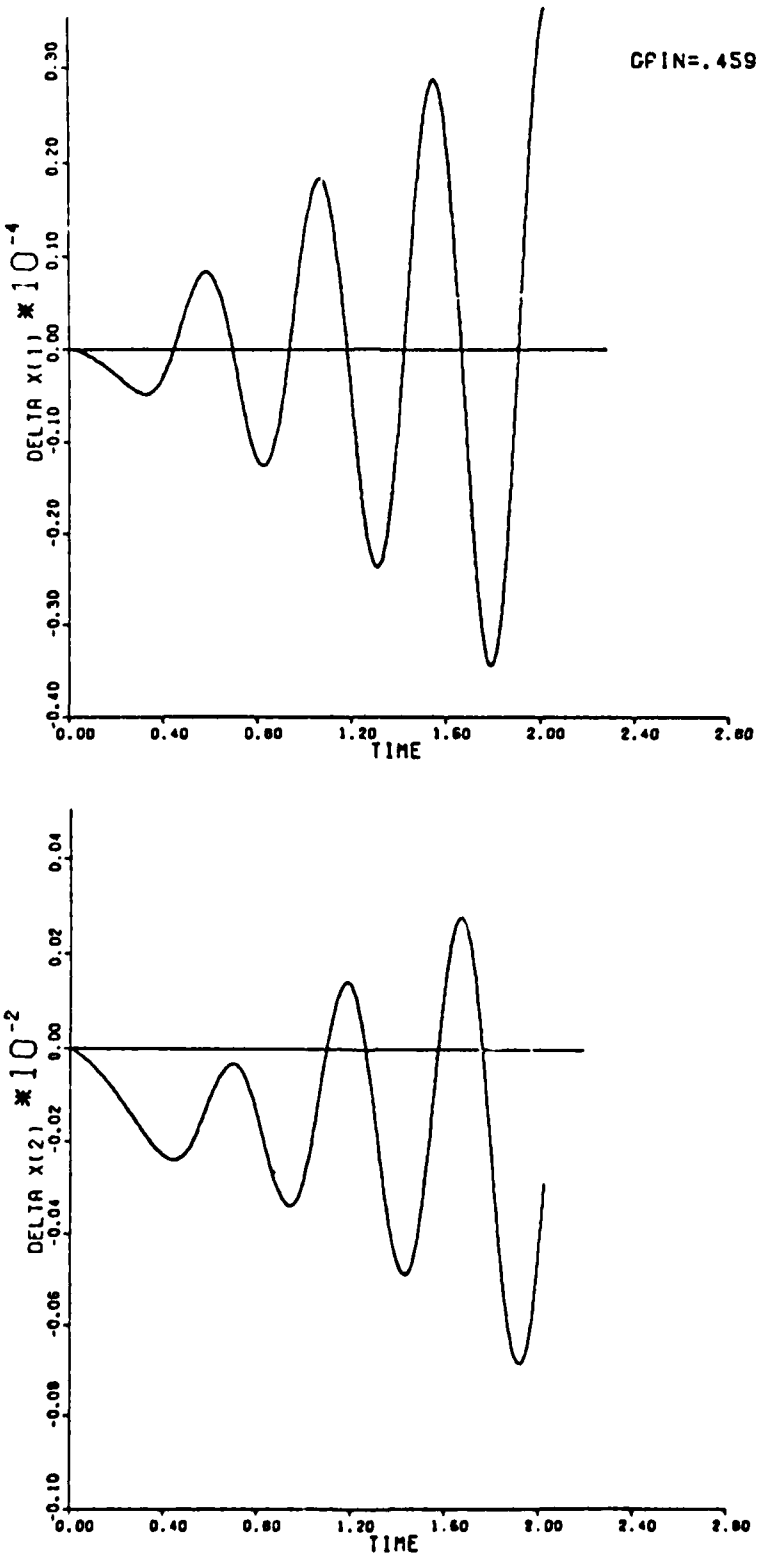

Figure 25. δx_1 and δx_2, Lunar Inclination and Eccentricity Effects Included (4 orbits)

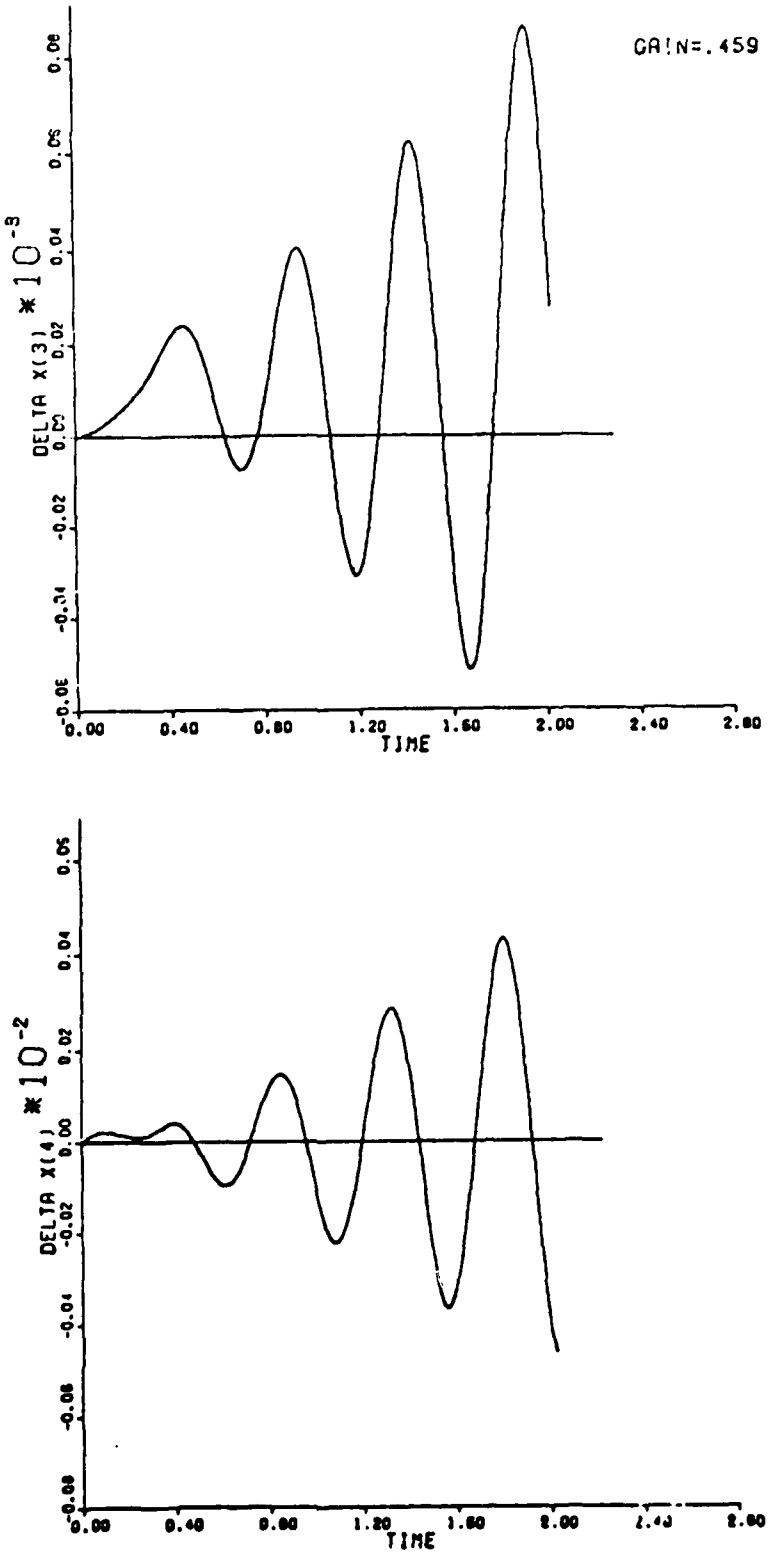

Figure 26. δx_3 and δx_4, Lunar Inclination and Eccentricity Effects Included (4 orbits)

This equation was then integrated along with the other six equations of motion to form an integrated control cost. At the end of the four month period of operation, the control cost for the case described by Figures 24-27 was 1.026×10^{-6} m/sec^2 which is, after conversion, an average acceleration of 1.047×10^{-7} g. By comparison, Farquher (Ref 3:63) cites earth-synchronous satellite control costs of 1.51×10^{-7} g.

Conclusions

As evidenced by Figures 9 and 10, the controller does exhibit predicted theoretical behavior by driving η_3 and η_4 to zero and not affecting η_1 or η_2. The oscillations present in the behavior of the modes for longer runs are not, therefore, induced by the controller. Two possibilities have been postulated for the oscillatory modal behavior. As previously stated, since the reference periodic orbit about L3 was constructed in single precision arithmetic with an integrator accurate to 10^{-10}, and then represented by a Fourier series (an approximation technique when the Fourier series is truncated), it is possible that the reference orbit inaccuracies caused the reference orbit to be out-of-sync with the actual integrated and controlled orbit. The other possibility is that the moon's orbit creates the oscillations seen on the plots. In all cases, the period of the oscillations was approximately the L3 orbital period which is also the period of the moon's orbit. In

the case of the plots of η_1 and η_2 for the different cases, it appears that the periodic forcing function of the moon is modulating the underlying predicted (and observed) sine wave. For η_3 and η_4, the same forcing function appears superimposed on the predicted exponentials. If the lunar orbit does, in fact, cause the oscillations, the oscillations can be viewed as a result of resonance between the lunar and L3 orbits.

The control cost cited for the case shown by Figures 23-26 was 31 percent lower than the costs incurred by satellites in synchronous orbits. Since control costs were the primary yardstick for feasible of modal control, one concludes that modal control is a viable scheme. The orbit about L3 provides an excellent location for sensor-bearing satellites, particularly when coverage of the polar regions is of paramount importance. One can also state that the same control technique could be applied to satellites in orbits about L4 and L5, providing the desired total global coverage.

Recommendations

Follow-on studies should construct the periodic reference orbit about L3 with double precision arithmetic to insure the out-of-sync condition mentioned previously does not exist or is minimized. The resonance condition (if it exists) is a function of the dynamics of the problem and therefore must be tolerated.

A further attempt to alleviate the oscillation (ringing) problem would be to use some sort of state estimation technique rather than the purely deterministic dynamics of this study. State estimation should cure any frequency mismatch problems that might exist and provide an easy vehicle for optimizing the control law. State estimation techniques have been used extensively in the studies of control of large space structures and the theory should directly apply to this problem.

Since the Poincare exponents of one planar mode and the out-of-plane mode are purely imaginary, one can only say that they are marginally stable. Control theory predicts pure oscillation for roots on the imaginary axis and the expected oscillatory motion for these modes does, in fact, occur. Future studies should investigate adding damping to these modes to move the roots off the imaginary axis and into the left-half of the complex plane, thereby producing stable modes rather than marginally stable modes.

Bibliography

1. Bate, R.R., Mueller, D.D., and White, J.E., Fundamentals of Astrodynamics, New York: Dover Publications, 1971.

2. Brouwer, D. and Clemence, G.M., Methods of Celestial Mechanics, New York: Academic Press, 1961.

3. Farquher, R.W., "The Control and Use of Libration Point Satellites", NASA Technical Report R-346, 1970.

4. Hartman, P., Ordinary Differential Equations, New York: John Wiley & Sons, 1964.

5. Heppenheimer, T.A., "Steps Toward Space Colonization: Colony Location and Transfer Trajectories." Journal of Spacecraft and Rockets, 15:305-12 (1975).

6. Jones, J.F., Kroncke, G.T., Vermaire, P.J. and Willett, D.A., Course Text, Astronautics 332, Dept. of Astronautics and Computer Science, U.S. Air Force Academy, CO.

7. Meirovitch, L., Methods of Analytical Dynamics, New York: McGraw-Hill, 1970.

8. Smith, D.E., "Stabilizing an Unstable Orbit About L3 in the Sun, Earth, Moon System Using Linear Constant Gain Feedback", Master's Thesis, Wright-Patterson AFB, OH: A.F. Institute of Tech, 1979.

9. Szebehaly, V., Theory of Orbits: The Restricted Problem of Three Bodies, New York: Academic Press, 1967.

10. Wiesel, W.E., "Floquet Reference Solutions for the Lunar Theory and Jovian Moon System", American Institute of Aeronautics and Astronautics Paper 80-1655.

Vita

William L. Shelton was born February 25, 1954, in Tulsa, Oklahoma. In April, 1963, he and his family moved to Oklahoma City where he attended Moore, Oklahoma schcols. He graduated from high school in May, 1972 and entered the U.S. Air Force Academy in July, 1972. He graduated from USAFA in 1976 with a Bachelor of Science degree in Astronautical Engineering.

In August, 1976, Shelton was assigned to the 6595th Missile Test Group at Vandenberg AFB, California, and there spent two years assisting in the launches of Minuteman I ICBMs with experimental reentry vehicles for payloads. He then served for one year as the Technical Assistant/Aide to the Commander of the Space and Missile Test Center at Vandenbert AFB.

In June, 1979, Shelton was reassigned to the Air Force Institute of Technology School of Engineering at Wright-Patterson AFB, Ohio and he began studies toward a Master of Science degree in Astronautical Engineering, Guidance and Control. After graduation, Shelton will be assigned to NASA's Lyndon B. Johnson Space Center in Houston, Texas and will work in the Guidance, Navigation, and Control Section of the Flight Operations Division.

Shelton is married to the former Linda Marical of Moore, Oklahoma.

Permanent Address: 9813 Henderson Drive
Oklahoma City, OK 73139

SECURITY CLASSIFICATION OF THIS PAGE (When Data Entered)

REPORT DOCUMENTATION PAGE		READ INSTRUCTIONS BEFORE COMPLETING FORM
1. REPORT NUMBER AFIT/GA/AA/80D-3	2. GOVT ACCESSION NO. AD-A094 812	3. RECIPIENT'S CATALOG NUMBER
4. TITLE (and Subtitle) MODAL CONTROL OF A SATELLITE IN ORBIT ABOUT L3		5. TYPE OF REPORT & PERIOD COVERED MS Thesis 6. PERFORMING ORG. REPORT NUMBER
7. AUTHOR(s) William L. Shelton Captain, USAF		8. CONTRACT OR GRANT NUMBER(s)
9. PERFORMING ORGANIZATION NAME AND ADDRESS Air Force Institute of Technology (AFIT/EN) Wright-Patterson AFB, OH 45433		10. PROGRAM ELEMENT, PROJECT, TASK AREA & WORK UNIT NUMBERS
11. CONTROLLING OFFICE NAME AND ADDRESS		12. REPORT DATE December, 1980 13. NUMBER OF PAGES 81
14. MONITORING AGENCY NAME & ADDRESS(if different from Controlling Office)		15. SECURITY CLASS. (of this report) 15a. DECLASSIFICATION DOWNGRADING SCHEDULE

16. DISTRIBUTION STATEMENT (of this Report)

Approved for public release; distribution unlimited

17. DISTRIBUTION STATEMENT (of the abstract entered in Block 20, if different from Report)

18. SUPPLEMENTARY NOTES

Approved for public release, IAW AFR 190-17
FREDERIC C. LYNCH, Major, USAF
Director of Public Affairs
Air Force Institute of Technology
30 DEC 1980

19. KEY WORDS (Continue on reverse side if necessary and identify by block number)

Periodic Orbits
Lagrange Points
L3
Modal Control
Floquet Theory

20. ABSTRACT (Continue on reverse side if necessary and identify by block number)

A modal control scheme was developed for linear systems that are time periodic. The scheme was then applied to a satellite in orbit about the earth-moon Lagrange point, L3. A theoretical control gain prediction was also devised and then verified by numerical results. The feasibility of the control scheme was demonstrated by computer simulations by controlling the actual nonlinear equations of the satellite with the linearly derived control. The satellite control costs were found to be

DD FORM 1473 EDITION OF 1 NOV 65 IS OBSOLETE

SECURITY CLASSIFICATION OF THIS PAGE (When Data Entered)

30 percent less than the control costs of a satellite in earth-synchronous orbit.

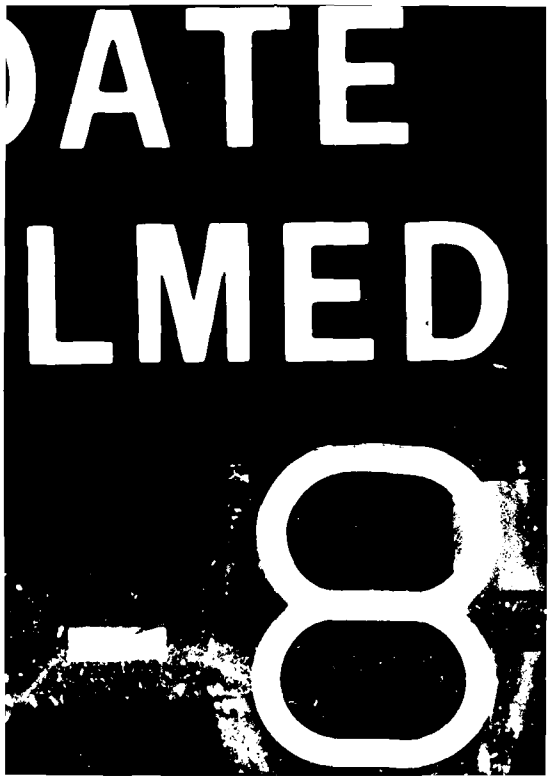
ATE
LMED
8